

## Depositional environment, geochemistry and diagenetic control of the reservoir quality of the Oligo-Miocene Asmari Formation, a carbonate platform in SW Iran

Armin OMIDPOUR<sup>1</sup>, Reza MOUSSAVI-HARAMI<sup>1, \*</sup>, A.J. (Tom) VAN LOON<sup>2</sup>, Asadollah MAHBOUBI<sup>1</sup> and Hossain RAHIMPOUR-BONAB<sup>3</sup>

<sup>1</sup> Ferdowsi University of Mashhad, Department of Geology, Faculty of Sciences, Azadi Square, Mashhad, Razavi Khorasan Province, Iran

<sup>2</sup> Shandong University of Science and Technology, College of Earth Science and Engineering, Qingdao 266590, Shandong, China

<sup>3</sup> University of Tehran, School of Geology, College of Science, 16th Azar Street, Enghelab Square, Tehran, Iran

Omidpour, A., Moussavi-Harami, R., Van Loon, A.J. (Tom), Mahboubi, A., Rahimpour-Bonab, H., 2021. Depositional environment, geochemistry and diagenetic control of the reservoir quality of the Oligo-Miocene Asmari Formation, a carbonate platform in SW Iran. *Geological Quarterly*, 2021, 65: 27, doi: 10.7306/gq.1596



The Oligo-Miocene Asmari Formation in SW Iran represents sedimentation on a carbonate platform. Thin-section analysis allowed distinguishing 26 microfacies, which can be grouped into twelve microfacies associations that represent four main depositional environments: open-marine, outer-ramp, middle-ramp and inner-ramp settings. The carbonates have undergone a complex diagenetic history, from pencontemporaneous shallow-marine consolidation to deep-burial diagenesis. The most important processes that affected the carbonates are dolomitization (in different stages), cementation (by anhydrite and calcite), dissolution (fabric-selective and fabric-destructive), fracturing, stylolitization and neomorphism. Minor diagenetic processes that modified the sediments are pyritization, silicification, glauconitization, micritization and bioturbation. Diagenetic processes such as dolomitization, dissolution and fracturing improved the reservoir quality, whereas cementation and compaction have reduced the reservoir quality of the Asmari Formation. Whole-rock oxygen and carbon isotope analyses of limestone samples show that the isotopic composition of the carbonates was hardly affected by diagenesis and that the carbonates remained roughly in isotopic equilibrium with the Paleogene seawater. Some samples have, however, been affected significantly by diagenesis during deep burial in a closed to semi-closed diagenetic system.

Key words: Asmari Formation, Shadegan Oil Field, reservoir geology, diagenesis, oil exploration.

### INTRODUCTION

The most important applications of geochemical studies in carbonate rocks are identifying the precursor carbonate mineralogy, sedimentary environment, and the evaluation of palaeotemperature and palaeoclimate. In addition, such studies are currently used for palaeosalinity reconstruction, demonstrating diagenetic alteration rates, distinguishing between various diagenetic environments (marine, meteoric, burial), and recognizing diagenetic trends (e.g., Rao, 1996; Immenhauser et al., 2002; Vincent et al., 2006; Adabi and Mehmandosti, 2008).

Carbonate minerals in marine settings are potentially ideal targets for geochemical studies (Hood et al., 2018) because of the commonly limited influence of detrital components, and because carbonates tend to preserve their petrographical and geo-

chemical characteristics during alteration and lithification. Compared to the parent solution (the seawater), such minerals are, when precipitated from seawater at low temperatures, more enriched in <sup>18</sup>O than minerals formed at higher temperatures. This leads to a higher  $\delta^{18}\text{O}$  value. This parameter is therefore not only important because it makes it possible to distinguish marine carbonates from minerals precipitated from meteoric water (which generally show lower values of  $\delta^{18}\text{O}$ ), but also because stable-isotope and elemental data of carbonate rocks can be used to evaluate palaeotemperature and palaeoclimate by reconstructing the chemical and isotopic content of the ancient seawater and/or diagenetic fluids (e.g., Tucker and Wright, 1990; Lear et al., 2000; Crowe et al., 2013; Swart, 2015; Fallah-Baghtash et al., 2020). The various geochemical (including isotopic) data are commonly interpreted with the help of cross-plot diagrams, as these facilitate detection of diagenetic signals.

The present contribution deals with the Oligocene-Miocene Asmari Formation, a stratigraphic unit which hosts numerous supergiant and giant hydrocarbon accumulations that contain >90% of the recoverable oil of Iran (Ghazban, 2007). Integrated geochemical analyses (stable isotopes of carbon and oxygen, as well as trace elements) and petrographic studies have been

\* Corresponding author, e-mail: [moussavi@um.ac.ir](mailto:moussavi@um.ac.ir)

Received: November 6, 2020; accepted: April 12, 2021; first published online: May 26, 2021

carried out to increase the insight into carbonate diagenesis (e.g., Swart, 2015; Hood et al., 2018). Such studies show that diagenetic processes in carbonates may include modifications of texture, mineralogy, chemistry, and porosity, and thus significantly affect reservoir quality. The present study of the Asmari Formation is based on a combination of core analysis, thin-section petrography and trace-element and stable-isotope analysis. The main objective of the study is to recognize the effects of diagenetic processes that affected the Oligo-Miocene carbonates on their quality as oil reservoirs.

## GEOLOGICAL SETTING

The Shadegan Oil Field is located in the southwestern part of the Dezful Embayment, within the Zagros Basin (Fig. 1A). The Zagros region is one of the important tectono-stratigraphic domains in southwestern Iran. Its approximate length is >1600 km and its width is 200-250 km (Sherkati and Letouzey, 2004; Heydari, 2008). The main trend in this huge geotectonic structure, which forms part of the Alpine-Himalayan orogenic belt (Alavi, 2004), is NW–SE, starting in SE Turkey and extending to the Hormuz Strait (Sherkati and Letouzey, 2004).

The Zagros Basin was formed due to the closure of the Neo-Tethys Ocean during convergence and eventual collision between the Arabian Plate (from the north-east) and the Central Iran/Eurasian Plate (Alavi, 2004; Navabpour and Barrier, 2012). The present-day morphology of the Zagros Mountains is the result of two main compressive phases: a first phase with subduction to the NE and obduction in the Late Cretaceous (Saura et al., 2011), and a second phase with collision during the Neogene (Sherkati and Letouzey, 2004; Lashgari et al., 2020). The Oligocene-Miocene Asmari Platform was formed mainly during the final stage of the closure of the Neo-Tethys Ocean and the beginning of a foreland development (Sherkati et al., 2006).

Based on its tectonic activity and depositional history, four tectono-stratigraphic zones can be distinguished in the Zagros Basin. They are, from NW to SE (Fig. 1A), Lurestan, the Dezful Embayment, the Izeh Zone and Fars (Heydari, 2008). The present study deals with a region in the Dezful Embayment, which covers ~7000 km<sup>2</sup> and is surrounded by three major faults: the Mountain Front Fault, the Balarud Fault, and the Kazerun Fault (Sepehr and Cosgrove, 2004; Saura et al., 2015; Fig. 1A). This embayment hosts almost all major Iranian oil fields (Bordenave and Hegre, 2010).

The subject of the present study, the Shadegan Oil Field, is located in the south-western part of the Dezful Embayment, ~60 km SE of the city of Ahwaz. It is a high-relief, asymmetric anticline of 23 km long and 6 km wide, situated at 30°05' to 31°00'N and 49°06' to 49°15'E (Fig. 1B). The petroliferous Oligocene-Miocene Asmari Formation in the Shadegan Oil Field consists mainly of cream- to brown-coloured limestones and porous dolostones alternating with shales (Fig. 2). It conformably overlies the marly and shaly Pabdeh Formation and is, in turn, conformably overlain by the evaporites of the Gachsaran Formation.

## MATERIAL AND METHODS

The present study is based mainly on the analysis of rock samples from the Asmari Formation, collected at core intervals from five boreholes (SG-4, SG-7, SG-8, SG-11 and SG-12) in the Shadegan Oil Field (Fig. 3). The thickness of the formation ranges in these boreholes between ~363 and 390 m. The lime-

stone types have been classified according to the schemes of Dunham (1962), and Embry and Klovan (1971), and the dolomites have been classified following Sibley and Gregg (1987). From the core samples, 1123 thin-sections were prepared; these were stained with potassium ferricyanide and Alizarin Red S to distinguish the various types of carbonate minerals (cf. Dickson, 1965).

Forty-eight limestone and thirty-two dolomite samples from the cores were carefully powdered, using a small drill, and the powdered samples were analysed for several major and trace elements. Elemental analysis was performed by atomic absorption spectrophotometry (AAS) at the central lab of Ferdowsi University of Mashhad, Iran. The accuracy of these analyses was better than ±5 ppm for Mn, Fe, Sr, and Na, and 0.5% for Mg.

The forty-eight powdered limestone samples were first analysed for their major and trace elements, and subsequently for their oxygen and carbon isotopes at the G.G. Hatch Stable Isotope Laboratory, University of Ottawa; this was done with a VG STRA Series II apparatus. The samples were weighed in containers, and 0.1 mL of H<sub>3</sub>PO<sub>4</sub> (specific weight 1.91) was added to the side. Then the containers were capped, placed in a horizontal position, and flushed with helium. The resulting reaction of calcite (at 25°C) during 24 hours was followed by extraction in continuous flow. The measurements were performed with a Delta XP and a Gas Bench II, both from Thermo Finnegan. The analytical precision (2 σ) was ±0.1‰. The oxygen and carbon isotope values are reported relative to the Vienna PeeDee Belemnite (VPDB) standard.

## DEPOSITIONAL ENVIRONMENTS AND MICROFACIES

Thin-section analysis of the carbonate samples, following – but adapting where necessary – the method introduced by Flügel (2010) resulted in the distinction of 26 microfacies. The detailed description of these microfacies, as well as their fossil content, is the subject of other studies (Avarjani et al., 2015; Omidpour et al., 2021). The present study focuses on the interpretation of the depositional environment and its sub-environments.

The 26 microfacies can be grouped into 12 facies associations, which represent specific depositional conditions that reflect depositional sub-environments. These sub-environments, in turn, represent four main environments: open-marine, outer ramp, middle ramp and inner ramp. The ramp was most probably of a homoclinal type as indicated by the absence of large barrier reefs (Avarjani et al., 2015; Omidpour et al., 2021), although small reefs are present, commonly as patches. The microfacies, which are distinguished and interpreted for a considerable part on the basis of their bioclast content, pass gradually into each other.

### OPEN-MARINE ENVIRONMENT

The open-marine environment is represented by only one microfacies, formed by alternations of marls and shales. They represent low-energy conditions that are interpreted, also on the basis of their wide, continuous extent, as formed by settling in an open-marine environment. Trace fossils such as *Cylendrichnus*, *Thalassinoides*, *Rossetina*, and *Nereites* indicate a low sedimentation rate. In spite of the overall quiet conditions, some (probably slow) bottom currents may have been present considering the occasional presence of small, rounded dolomite grains.

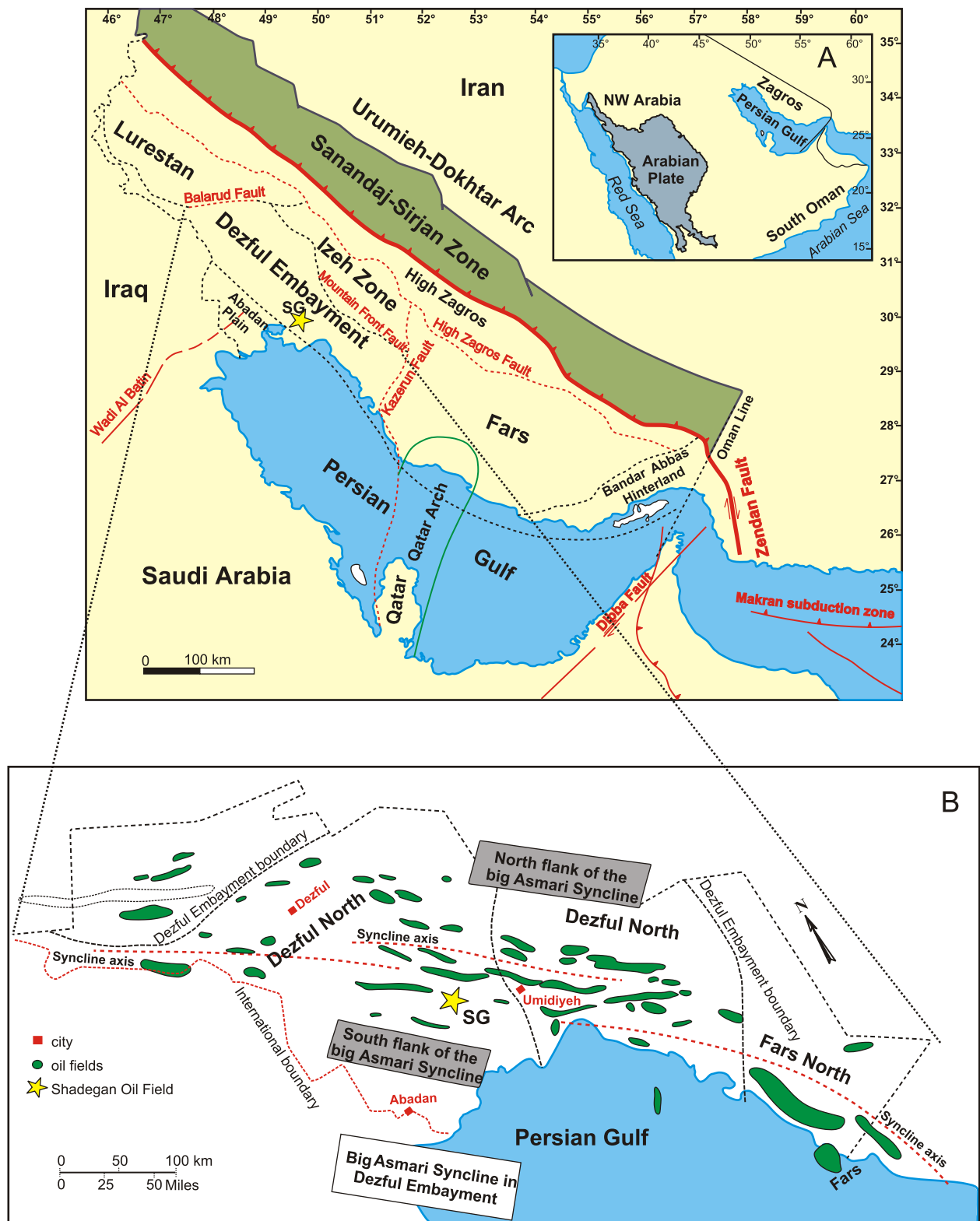


Fig. 1. Location maps of the study area

A – regional map showing the main structural elements in SW Iran (after Sharland et al., 2004);  
 B – location of the Shadegan Oil Field in the Dezful Embayment of the Zagros Basin

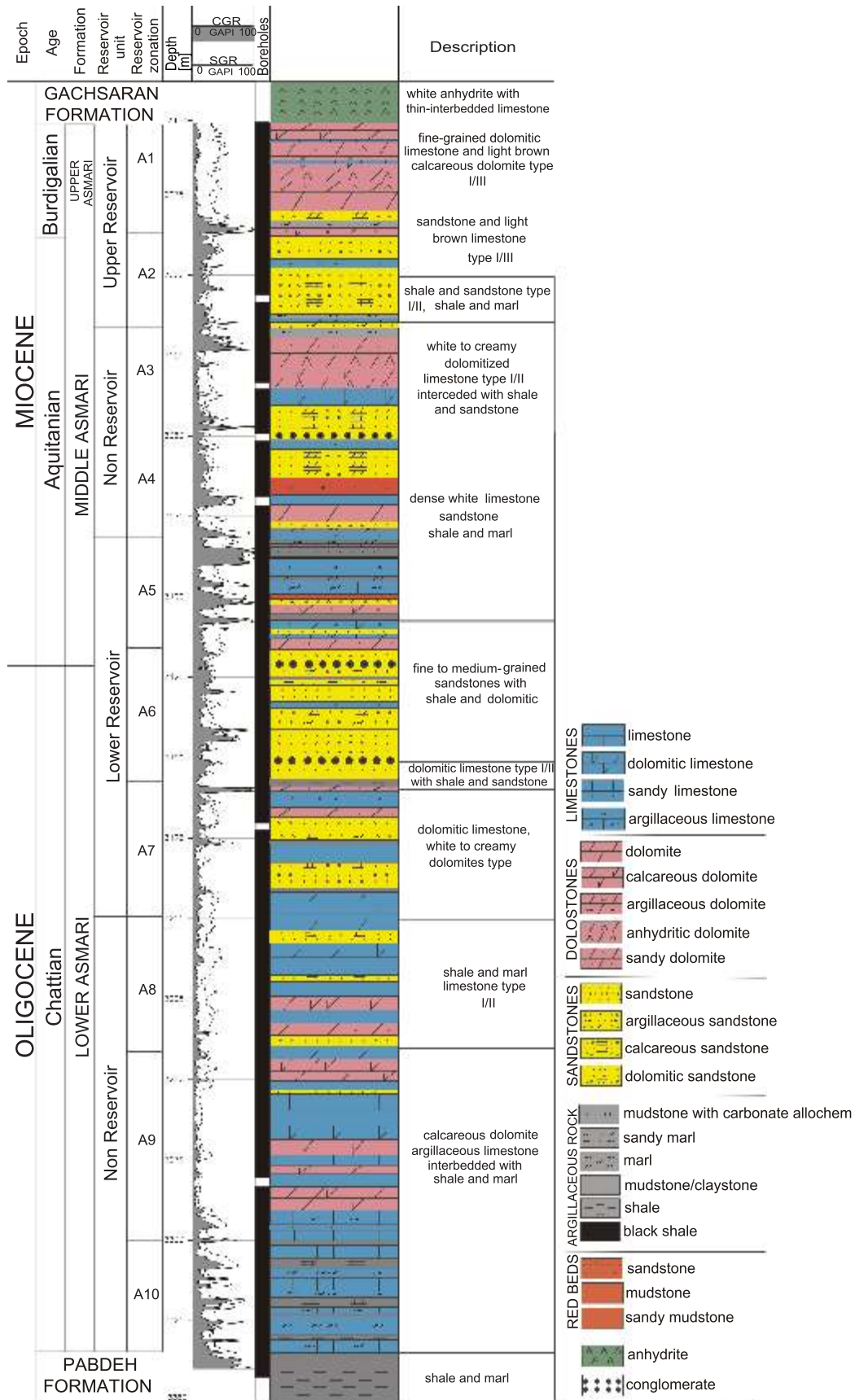


Fig. 2. Type section (subsurface) of the Oligo-Miocene Asmari Formation in borehole SG-11

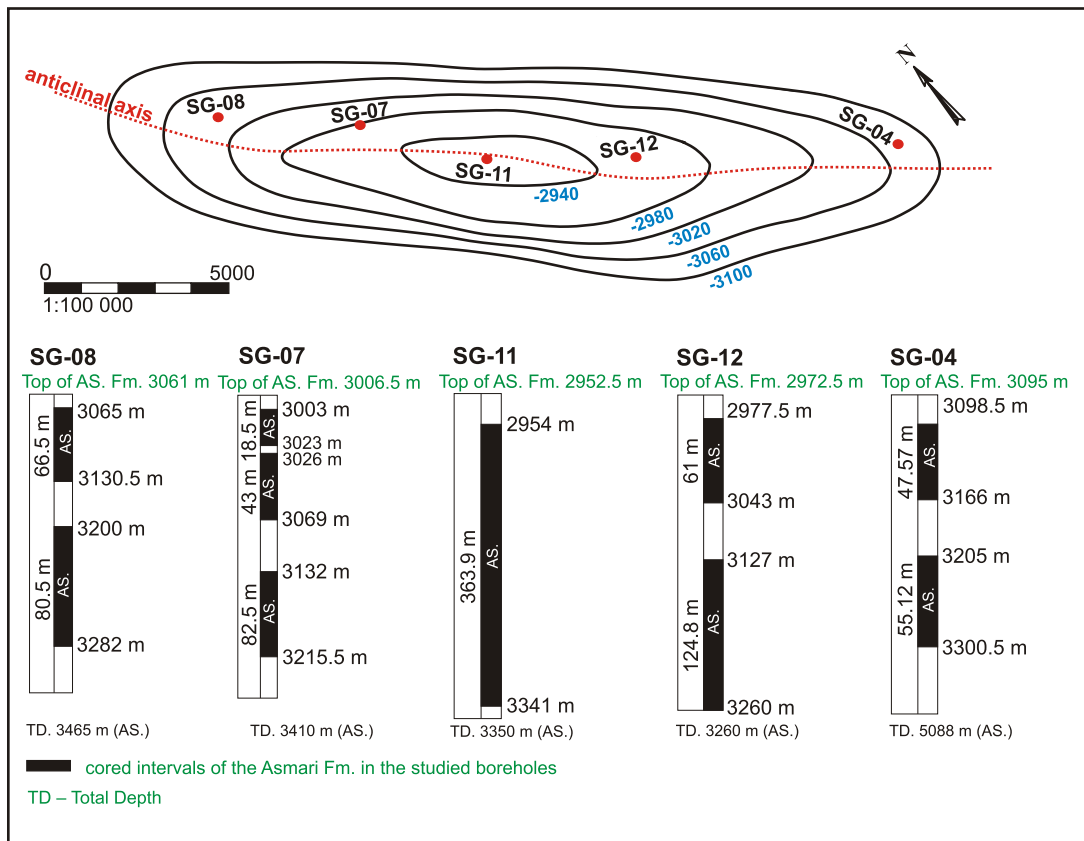


Fig. 3. The Asmari reservoir

**A** – contour map showing the depth (in m) of the top of the Asmari reservoir and locations of the five boreholes in the Shadegan Oil Field mentioned in this study; **B** – cored intervals of the five boreholes (SG-4, SG-7, SG-8, SG-11 and SG-12) in the Shadegan Oil Field

#### OUTER RAMP

The outer ramp shows the gradual transition from the truly open-marine setting to a platform realm. This is expressed in the form of two sub-environments: a distal outer ramp and a proximal outer ramp. Both sub-environments had a moderate energy level.

The distal outer-ramp sub-environment is characterized by a facies association constituted by two microfacies with a fauna consisting mostly of planktonic foraminifers and bryozoans. The two facies of this association are:

- alternations of bioclastic wackestones and mudstones,
- alternations of wackestones and floatstones that also contain large benthic foraminifers.

The presence of framboidal pyrite indicates that reducing conditions existed, at least occasionally, at or within the bottom, probably due to the high rate of accumulation of organic remains of planktonic fauna.

The proximal outer-ramp sub-environment is characterized by a facies association that also contains two microfacies, consisting of bioclastic rudstones with a matrix of wackestone, in which the fauna is dominated by large benthic foraminifers. The difference between the two microfacies of this association is that in one of them the large benthic foraminifers consist mainly of *Operculina*, whereas *Eulepidina* dominates the other microfacies.

#### MIDDLE RAMP

The middle ramp can be subdivided into three sub-environments (deep subtidal, shallow subtidal, and patch reefs), which represent the further transition from open-marine (with a transition to the outer ramp) to the inner ramp. The energy level was, as a result of the shallower setting and the consequently larger influence of waves, higher than on the outer ramp, ranging from moderate to high.

The deep subtidal part of the middle ramp is characterized by a microfacies association consisting of carbonates with a highly dolomitized matrix and significantly less dolomitized grains. The fauna was dominated by large benthic foraminifers. Moderate- to high-energy conditions prevailed. Two microfacies are present:

- alternating wackestones, packstones, and rudstones in which the large foraminifer *Lepidocyclina* dominates,
- packstones in which *Rotalia viennoti* prevails.

The shallow subtidal sub-environment, with its moderate to high energy level, consists of micrites, a muddy matrix, and syntaxial and isopachous rim cement. Benthic foraminifers (particularly miliolids) and gastropods are the most common fauna. Two microfacies can be distinguished:

- alternating wackestones, packstones and floatstones with echinoderms, red algae, and *Rotalia viennoti*,
- alternating wackestones and packstones with both imperforated and perforated foraminifers.

The patch reefs (and their erosional products) were built by corals, in addition to common echinoderms, coralline algae and the large benthic foraminifer *Rotalia viennoti*. The texture of the sediment is obviously controlled by the coral growth, but the high original porosity has been reduced by chemical compaction and cementation, commonly by dolomitic micrite. The energy level in the sub-environment was high. Three microfacies can be distinguished:

- grainstones (representing reef talus) with algae, echinoderms and *Rotalia viennoti*,
- alternations of boundstones and rudstones with echinoderms, algae and coralline algae,
- boundstones consisting of corals.

#### INNER RAMP

The inner ramp is the most varied depositional environment in the study area, with six sub-environments representing, respectively, shoals, an open lagoon, a restricted lagoon, the proximal part of a restricted lagoon, intertidal and supratidal settings. The energy levels range from low to high, depending on the sub-environment. These sub-environments thus represent the outer end of the total spectrum from open-marine (see open-marine environment) to the supratidal setting dealt with here.

The microfacies association representing the shoals reflects high-energy conditions; the sediments are, as a rule, strongly cemented, and they commonly contain micritized specimens of ooids and bioclasts. Three microfacies can be distinguished:

- grainstones consisting mainly of ooids,
- grainstones consisting mostly of ooids and common specimens of *Faverina*,
- bioclastic grainstones.

The open-lagoon microfacies association consists of two microfacies that were deposited under low- to moderate-energy conditions; they contain numerous micritized bioclasts. The two microfacies are:

- bioclastic packstones with red algae and echinoderms,
- packstones with a large diversity of imperforated foraminifers.

The microfacies association representing the restricted lagoon has three microfacies that are all characterized by low-energy depositional conditions, the common presence of micritized bioclasts and biogenetic structures created by organisms that produced burrows and borings. The three microfacies are:

- alternating wacke- and packstones with miliolids,
- alternating wacke- and packstones with the miliolid foraminifer *Dendritina rangi*,
- bioclastic wackestones.

The association representing the proximal part of the restricted lagoon, where also low-energy conditions prevailed (as indicated by the imperforated foraminifers), consists of two microfacies:

- peloidal wackestones with miliolids and *Dendritina rangi*,
- peloidal bioclastic wackestones with mainly imperforated foraminifers.

The intertidal part of the inner ramp represents low- to moderate-energy conditions, and the sediments consist largely of silt. They are commonly bioturbated, and peloids are commonly present. Two microfacies can be distinguished:

- peloidal wackestones with common intraclasts,
- mudstones which only show some roughly horizontal lamination.

The last microfacies association, representing the supratidal part of the inner ramp, is characterized by low-energy conditions. Two microfacies can be distinguished:

- fine (<2  $\mu\text{m}$ ) dolomicrites,
- anhydrites with a nodular or laminated appearance.

#### DEPOSITIONAL ENVIRONMENT

The depositional environments of the 26 carbonate microfacies differ, apart from their fossil content, mainly from each other by the high- to low-energy conditions and their depth (which determines the light penetration). The environmental interpretation is, obviously, also largely based on the fossils (including ichnofossils) that indicate specific conditions of their habitat.

The overall environment of the Asmari Formation is best described as a homoclinal ramp (Omidpour et al., 2021). This interpretation is supported by:

- high frequency of porcelaneous foraminifers,
- dominant faunal genera and, most importantly,
- gradual facies change from a tide-dominated low-energy environment to oolitic/bioclast-rich high-energy shoals with a high carbonate-mud production and pervasive marine cementation (cf. Rowlands et al., 2014; Jafari et al., 2020).

Additional evidence for the environmental interpretation is provided by the lack of tempestites/turbidites, and by the absence of a large, laterally continuous barrier reefs (Avarjani et al., 2015; Fig. 4). The wide tidal flat with evaporites and dolomitic facies suggests a marine setting with a hot and arid climate. Evaporitic carbonate ramps generally form at passive continental margins with very gentle slopes (Bádenas and Aurell, 2001).

The lower part of the Asmari Formation contains abundant planktonic foraminifers and large benthic foraminifers (such as *Operculina* sp. and *Eulepidina* sp.) within a homogeneous, massive micrite. This indicates low-energy conditions in the quiet, deep waters (below storm wave base) of an outer-ramp setting with normal salinity (cf. Brigaud et al., 2009; Flügel, 2010). The open-marine sediments are mainly composed of pelagic shales/marls.

The middle part of the Asmari Formation is characterized by the presence of both imperforate and perforate foraminifers (*Rotalia viennoti* sp. and *Lepidocyclus* sp.), echinoids, bryozoans, coralline red algae and coral colonies, which suggests an oligophotic zone with good oxygen circulation in a middle-ramp setting (cf. Corda and Brandano, 2003; Asprion et al., 2009).

The upper part of the Asmari Formation contains, as main biogenic and non-biogenic components of the inner-ramp setting, imperforate foraminifers (such as the miliolids, *Dendritina rangi* sp., *Peneroplis thomasi* Henson; *Austrotrillina* sp., *Meandropsina* sp., *Quinqueloculina* sp. and *Pyrgo* sp.), and red algae together with ooids, peloids, and intraclasts. *Miliolina* sp. is the dominant genus in all studied microfacies; it is an indicator of warm to temperate, shallow water (Gonera, 2012). *Peneroplis* sp., *Quinqueloculina* sp., *Triloculina* sp., *Elphidium* sp. and *Dendritina rangi* are widely developed in the lagoonal sub-environment of the Persian Gulf (Amao et al., 2016). *Miliolina*-dominated benthic foraminifer assemblages reflect a decreased circulation and probably low-oxygen or euryhaline conditions (Geel, 2000). The shoal microfacies association is characterized by well to moderately sorted ooids and rounded bioclasts, with pervasive evaporites (anhydrite) and calcite cement indicating high-energy conditions (cf. Sim and Lee, 2006).

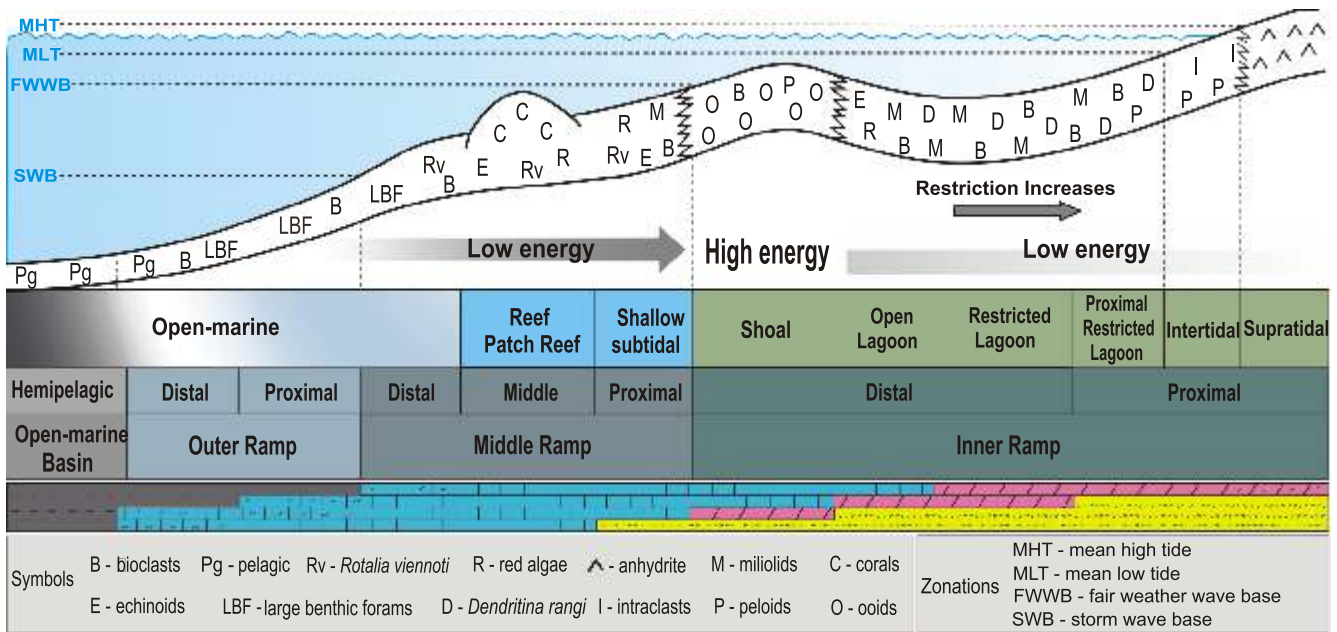


Fig. 4. Schematic depositional model of the homoclinal ramp upon which the Asmari Formation was deposited

For other explanations see Figure 2

### DIAGENETIC PROCESSES

The most important diagenetic processes in the Asmari Formation are micritization, compaction, cementation, dolomitization, dissolution, neomorphism and fracturing.

#### MICRITIZATION

Micritization represents the first diagenetic process affecting the limestones of the Asmari Formation. It occurred in several lithofacies, but particularly in mud-supported sediments. Complete micritization of grains led to the creation of peloids which preferentially occurred on foraminifers and algae, whereas micrite envelopes are common on shell fragments (Fig. 5A). These micritic envelopes are more resistant to dissolution than the grains, so they tend to be preserved after the total dissolution of grains. Subsequently, moulds were filled to varying degrees by coarse sparry calcite and later anhydrite cement.

Another process was the formation of accretionary micritic envelopes on large benthic foraminifers, particularly *Lepidocyclina* and *Operculina*, mainly in the lower part of the Asmari Formation (Fig. 5B).

#### COMPACTION

The compaction process strongly affected the characteristics of the Asmari reservoir rocks by reducing their porosity. During progressive burial of the formation, the increase in lithostatic pressure reduced the thickness of the sedimentary succession and resulted in a compact texture.

Evidence of this mechanical compaction is most distinct in lithofacies with a grain-supported texture (i.e., packstones and grainstones). Features indicating compaction are:

- broken allochems (Fig. 5C) and micrite envelopes (Fig. 5D) that show flattening, elongation, and re-orientation from their original positions to horizontal (Fig. 5E),
- squeezing of organic matter (Fig. 5F),
- concave/convex contacts of closely packed grains (Fig. 5G),
- ductile deformation and fracturing (Fig. 5H, I).

Moreover, grainstones may have formed by compaction of packstones by a closer packing of the grains (changing the ratio between framework grains and matrix), thus creating a grain-supported framework.

In addition to mechanical compaction, also chemical compaction took place, mostly in mud-dominated microfacies. The most common features are fitted fabrics, solution seams, and stylolites. Fitted fabrics are present as sutured contacts between skeletal fragments and between grains in fitted grainstones, mudstones, and wackestones (Fig. 6A). The stylolites developed parallel or sub-parallel to the bedding.

There are at least two stages of stylolitization. Stage I stylolites cross-cut muddy limestones, calcite cement, and dolomitic (Fig. 6B). Stage II stylolites cross-cut coarse crystalline dolomites but not saddle dolomite (Fig. 6C). The amplitudes of the stylolites vary from a few mm to a few cm; the contacts contain an insoluble residue of clay, organic matter, pyrite and hydrocarbons, which are opaque to translucent brown in thin-section. Solution seams occur in mudstones, wackestones and packstones, where they occur around and between particles (Fig. 6D).

#### CEMENTATION

The cements in the Asmari Formation are represented by aragonite, calcite and anhydrite.

Aragonite cement occurs as acicular (isopachous) rims in fibrous to radial forms (Fig. 6E), and as bladed isopachous rims.

Calcite cement occurs as peloidal micrite, meniscus (Fig. 6F), syntaxial overgrowths (Fig. 6G), and as equant (Fig. 6H), drusy (Fig. 6I), blocky, poikilitic (Fig. 6J), and coarse sparry

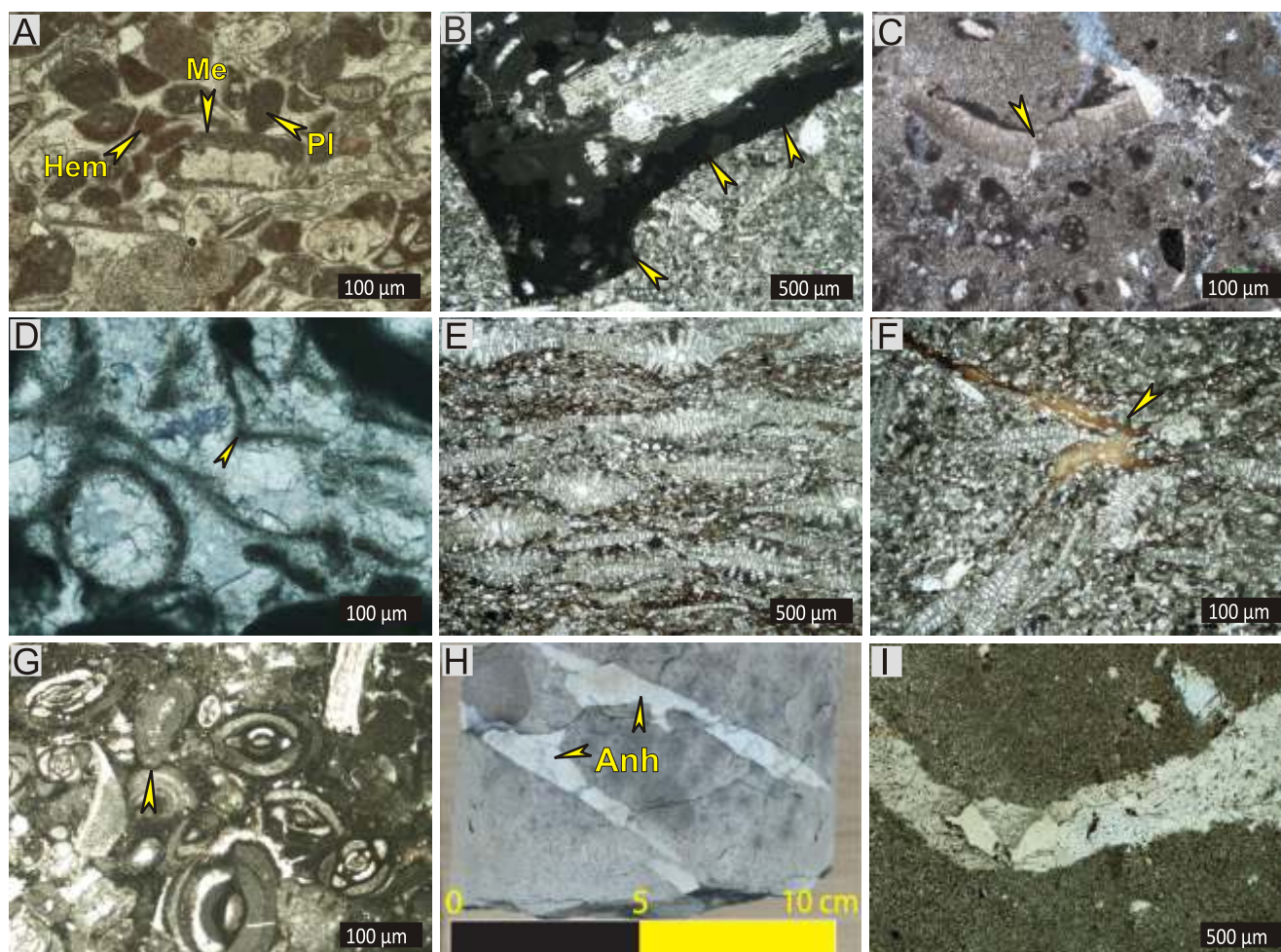


**Fig. 5. Micritization and mechanical compaction of the carbonates**

**A** – Peloids (PI) along with micrite envelopes (Me) on a shell fragment; some bioclasts are impregnated with iron oxide (Hem) (borehole SG-11, depth 3040 m); **B** – accretionary micritic envelope (yellow arrows) (borehole SG-11, depth 3303.34 m); **C** – broken allochem (yellow arrow) (PPL; borehole SG-04, depth 3232 m); **D** – broken micrite envelopes (yellow arrow) (XPL; borehole SG-04, depth 3207.3 m); **E** – re-orientation of *Lepidocyclus* specimens within a packstone (PPL; borehole SG-11, depth 3295.57 m); **F** – compaction of organic matter (yellow arrow) and *Lepidocyclus* (PPL; borehole SG-11, depth 3109 m); **G** – close packing of foraminifers with a convex/concave contacts (yellow arrow) (PPL; borehole SG-11, depth 3109 m); **H** – anhydrite (Anh) filling a fracture (arrow) during late burial (borehole SG-11, depth 3026.4 m); **I** – fracturing (borehole SG-11, depth 3016.6 m); thin-sections under plane polarized light (PPL) and crossed polars (XPL)

calcite. These forms may occur in all samples except for the most dolomitized microfacies. Some of the cements are Fe-bearing.

Anhydrite cement occupies a much larger part of the pore spaces than calcite cement. Anhydrite cementation was even the second most important diagenetic process after dolomitization. The first phase of anhydrite precipitation, in the form of replacement and cementation, took place during early diagenesis in upper intertidal and supratidal settings. A second phase of anhydrite formation, in the form of pervasive and fractures-filling cement, occurred during shallow to deep burial due to the infiltration of calcium-sulphate-bearing solutions that resulted from the migration of brines from the Gachsaran Formation into the porous, permeable Asmari Formation. These processes led to different types of layered anhydrite cement (Fig. 7A); thus cement may consist of sparse crystals (Fig. 7B), or be poikilotopic, pervasive (Fig. 7C), pore-filling, fracture-filling (Fig. 5H, I), vein-filling, or stylolite-filling.

## DOLOMITIZATION

Dolomitization is the most significant diagenetic process that has affected the Asmari carbonates; it occurred in all microfacies, though to varying degrees. Four types of dolomite crystals are present (for a detailed overview of the stratigraphic distribution of the various types of cement the reader is referred to Omidpour et al., 2021). The first type consists of very fine- to fine-crystalline dolomite (D1), which occurs mainly as anhedral crystals, commonly <10 μm in size, in the upper part of the succession (Fig. 7D, E). The second type is represented by fine- to medium-crystalline and mimic-replaced dolomite (D2), i.e. dolomite that preserves the precursor morphology (the primary morphology of bioclasts or non-skeletal grain) of replaced particles; it is present as planar, euhedral to subhedral crystals ranging from 30 to 50 μm, with a commonly unimodal crystal size distribution. This type is particularly present in the upper part of the succession, which most commonly formed in an inner-ramp en-

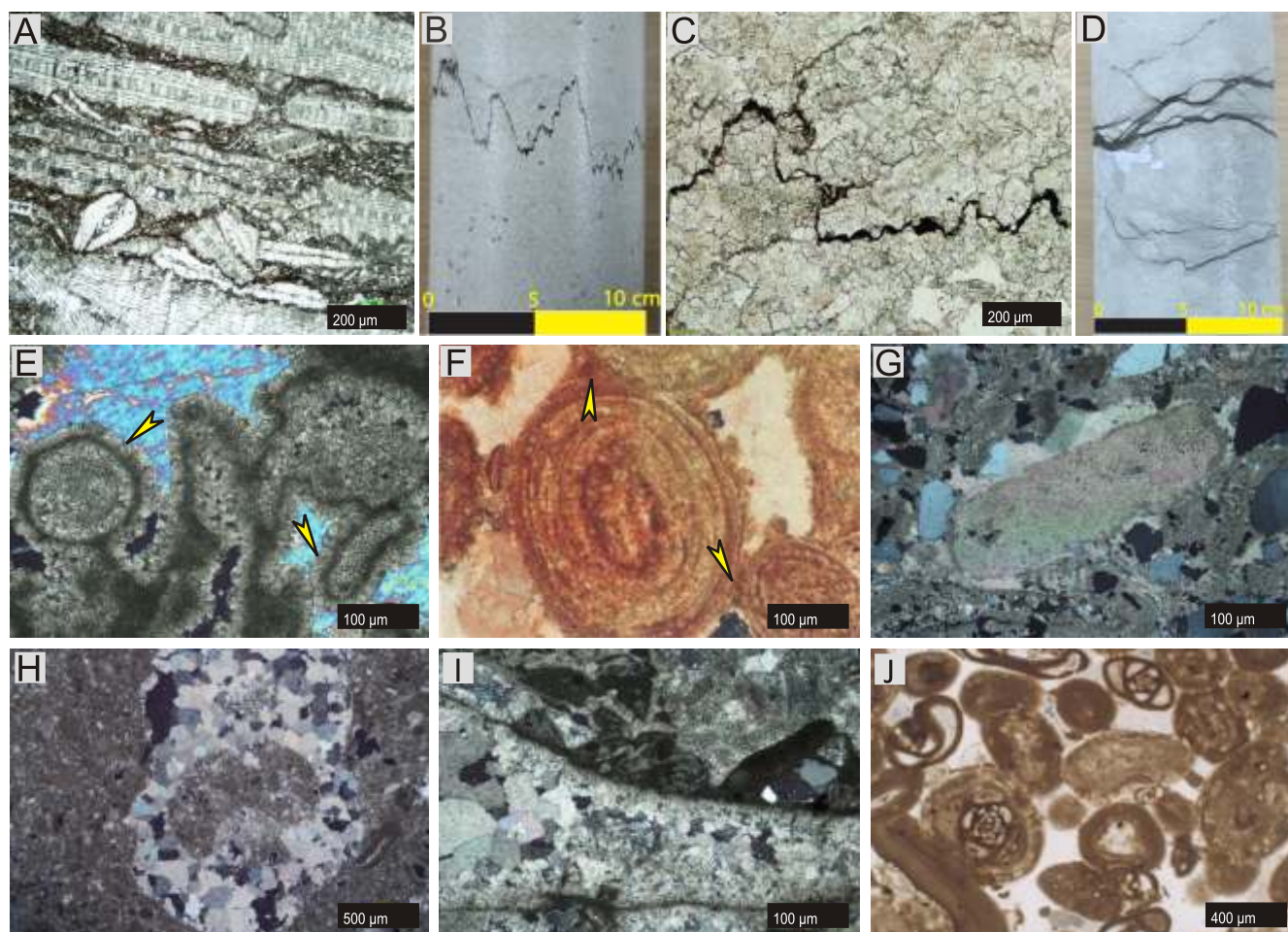


**Fig. 6. Chemical compaction and calcite cementation**

**A** – sutured contact between large benthic foraminifers (PPL; borehole SG-11, depth 3316.70 m); **B** – stage I stylolite (RS; borehole SG-04, depth 3207.75 m); **C** – solution seams (RS; borehole SG-04, depth 3109.75 m); **D** – stage II stylolite cross-cutting a coarse-crystalline dolomite, and containing an insoluble residue of clay, organic matter and hydrocarbons (PPL; borehole SG-04, depth 3285.57 m); **E** – acicular rim (isopachous) cement (yellow arrows) (PPL; borehole SG-08, depth 3088.45 m); **F** – meniscus cement (yellow arrow) (PPL; borehole SG-11, depth 3201.01 m); **G** – syntaxial overgrowth cement (XPL; borehole SG-11, depth 3207 m); **H** – equidimensional (granular mosaic) calcite cement (XPL; borehole SG-12, depth 3198 m); **I** – drusy calcite spar cement (XPL; borehole SG-12, depth 3222 m); **J** – poikilotopic calcite cement (PPL; borehole SG-11, depth 3205 m); thin-sections under plane polarized light (PPL) and crossed polars (XPL), and rock slabs (RS)

vironment (Fig. 7F, G). Some of them are Fe-bearing dolomite. The third type consists of medium- to coarse-crystalline dolomite with a destroyed fabric (D3), i.e. a dolomite with non-mimic replacement texture, resulting in destruction of the primary sedimentary structures, so that relicts of the original micrite and bioclasts are present only as ghost structures. The crystals are subhedral to anhedral with planar, non-planar, curved, lobate, or serrated intercrystalline boundaries (Fig. 7H). The crystals are 80–200 μm large and show a weak undulatory extinction. They occur scattered all over the succession. The fourth type, coarse-crystalline saddle dolomite (D4), is present as a creamy, white, or red cement. The crystals are non-planar, with partially or completely occluded vugs, moulds, and fractures (Fig. 7I). They range in size from 250 μm to 3 mm. Volumetrically, this type is fairly insignificant.

#### DISSOLUTION

Dissolution started during shallow burial and continued during the deep burial of the carbonates. The dissolution was com-

monly selective, and occasionally completely destroyed the original fabric of the sediment. Bioclasts of gastropods and foraminifers (originally composed of aragonite and high-Mg calcite) were selectively dissolved already during penecontemporaneous diagenesis, leaving voids that were later filled with sparry calcite, pore-filling anhydrite, or dolomite cement (Fig. 8A, B) that formed under either meteoric or shallow to intermediate burial conditions.

Micrite envelopes around bioclasts helped to preserve their original structures (Fig. 5D). Most dissolution occurred during burial diagenesis, destroying the original fabric. This enhanced the reservoir quality (Fig. 8C).

#### NEOMORPHISM

Thin-section analysis shows that the most common type of aggrading neomorphism is the transformation of micrite into microspar (Fig. 8D), and pseudospar (Fig. 8E). This occurred mainly in mudstones and wackestones.

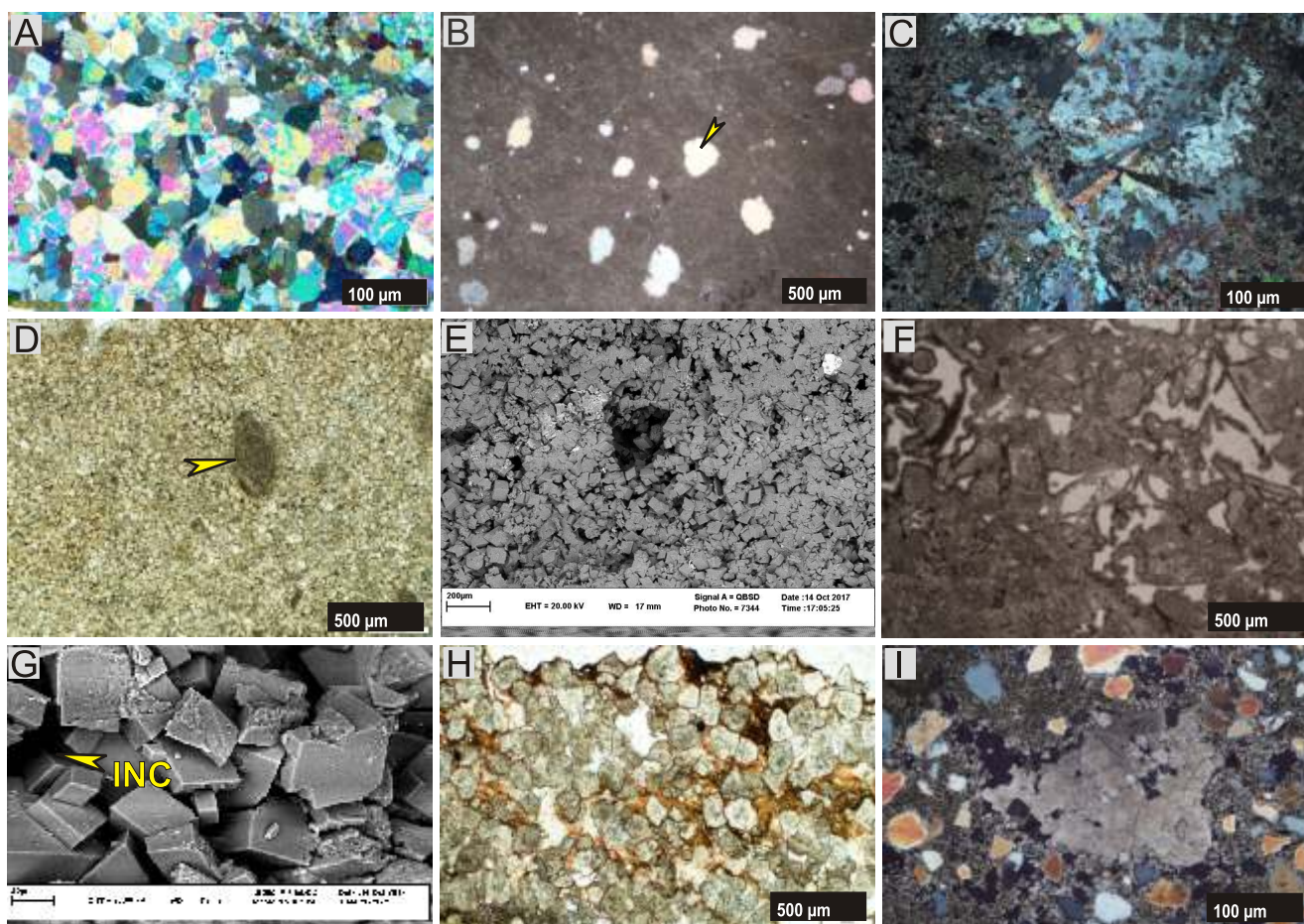


**Fig. 7. Main anhydrite and dolomite types**

**A** – supratidal anhydrite layer (XPL; borehole SG-11, depth 3034.25 m); **B** – sparse anhydrite crystals (yellow arrow) in dolomitic mudstone (XPL; borehole SG-07, depth 3031.5 m); **C** – pervasive anhydrite cement (XPL; borehole SG-11, depth 3299.05 m); **D** – very fine- to fine-crystalline dolomite (D1) with borehole-preserved precursor texture (yellow arrow) (PPL; borehole SG-12, depth 3222 m); **E** – very fine- to fine-crystalline dolomite (D1) (SEM); **F** – fine- to medium-crystalline fabric-retentive dolomite (D2) (PPL; borehole SG-11, depth 3035.12 m); **G** – fine- to medium-crystalline fabric-retentive dolomite (D2) (SEM); **H** – medium- to coarse-crystalline, fabric-destructive dolomite (D3) (PPL; borehole SG-11, depth 3225 m); **I** – large crystals of saddle dolomite (D4) (XPL; borehole SG-12, depth 3176 m); thin-sections under plane polarized light (PPL) and crossed polars (XPL), and SEM images (SEM)

The degrading neomorphism was caused mainly by recrystallization in a shallow subtidal setting (see section: MICRITIZATION). Therefore, this process occurred more frequently with decreasing distance to anticlinal axes. It is a rare diagenetic process in the Asmari Formation (Fig. 8F).

#### OTHER DIAGENETIC PROCESSES

Several other diagenetic processes have taken place, but they played only a minor role in the diagenetic alterations of the sediment.

Pyritization occurred through the replacement of dolomite with pyrite. The pyrite occurs as framboidal and cubic forms within dolomite. Glauconite was newly formed as light green euhedral crystals in the sediments of the middle and outer ramp (Fig. 8G). Authigenic quartz is a volumetrically minor component; it occurs mainly as a replacement of micrite matrix and early calcite cement (Fig. 8H), where it occludes pores.

In addition to the above-mentioned diagenetic processes, bioturbation also affected the sediments at the sedimentary

surface and in the form of burrowing; this occurred contemporaneously. This process occasionally obscured primary structures, particularly in the low-energy fine-grained lagoonal and open-marine microfacies. Borings into skeletal grains are also present (Fig. 8I).

#### INFLUENCE ON RESERVOIR QUALITY

The quality of the hydrocarbon reservoirs in the Asmari Formation depends largely on porosity and permeability. These parameters are largely controlled by diagenesis, rather than by sedimentology. Variations in porosity depend significantly on the presence (or absence) of dolomite.

Primary porosity is present in the limestones as fenestral, interparticle, and intraparticle porosity. Most pores have been occluded by early calcite cement, pore-filling anhydrite or lime mud.

Secondary porosity developed diagenetically after deposition. The secondary pores are by far the most abundant type of porosity and account for all reservoir porosity. More importantly,

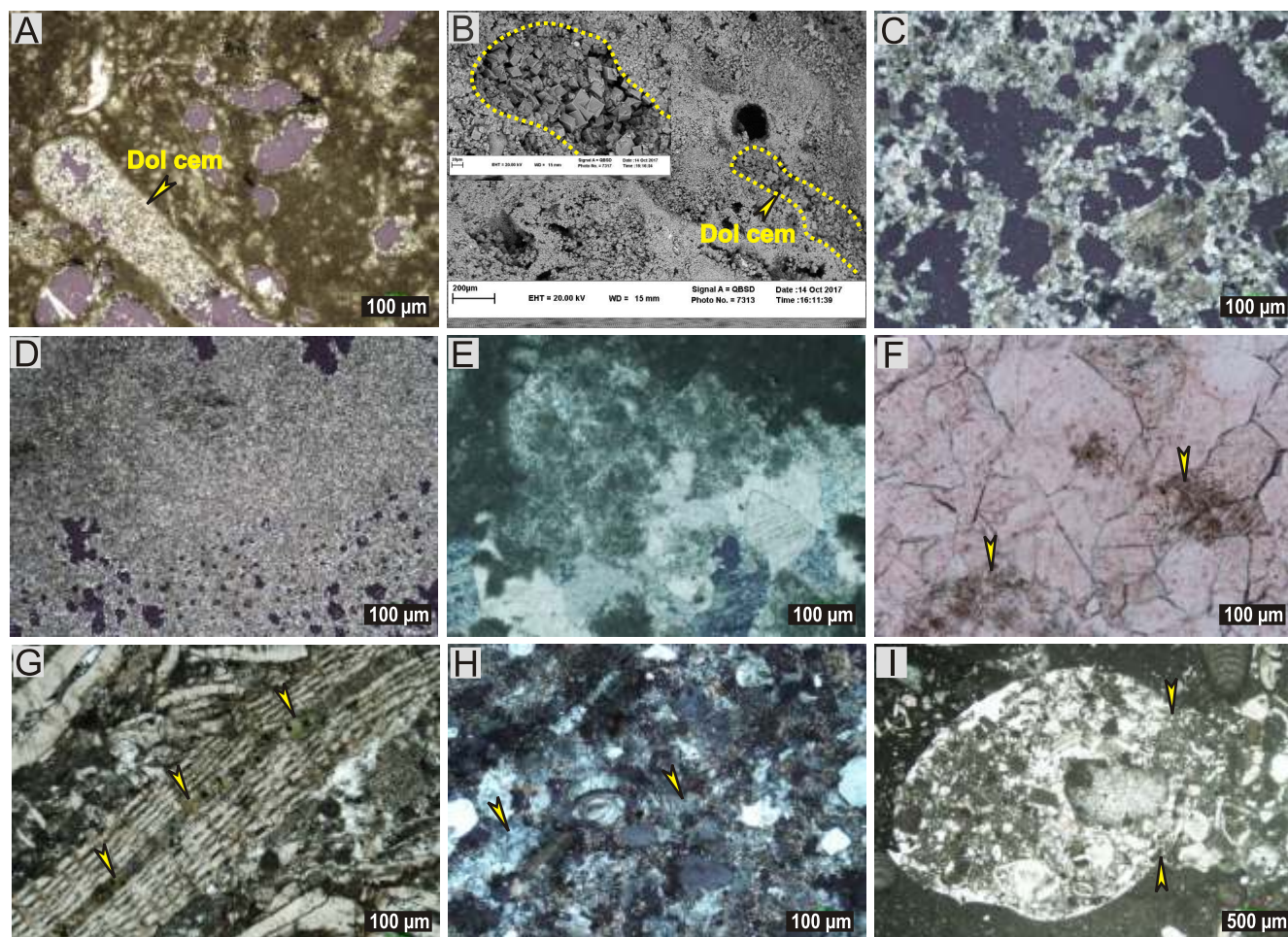


**Fig. 8. Dissolution, neomorphism and other diagenetic features**

**A** – fabric-selective dissolution during meteoric diagenesis (XPL; borehole SG-11, depth 3095.20 m); **B** – fabric-selective dissolution and dolomite cement (Dol cem) filling pores (SEM); **C** – fabric-destructive dissolution during late burial diagenesis (XPL; borehole SG-11, depth 3245.50 m); **D** – microspar (XPL; borehole SG-04, depth 3114.30 m); **E** – pseudospar (PPL; borehole SG-04, depth 3201 m); **F** – degrading neomorphism (yellow arrows) (PPL; borehole SG-12, depth 3198 m); **G** – authigenic glauconite (yellow arrows) (PPL; borehole SG-04, depth 3298.20 m); **H** – silicification (yellow arrows) (XPL; borehole SG-11, depth 3167.04 m); **I** – destruction by a boring organism (yellow arrows) (PPL; borehole SG-12, depth 3254.20 m); thin-sections under plane polarized light (PPL) and crossed polars (XPL), and SEM images (SEM)

secondary porosity is found in dolomitized limestones (Fig. 7F, G) as mouldic types (Fig. 8A, B), intercrystalline spaces (Fig. 7F, G), vuggy types, and fractures (Fig. 5H, I).

change the texture and composition of the original (precursor) rocks (Veizer, 1983). Isotopic and elemental analyses of carbonates help overcome this problem by identifying the precursor mineralogy of limestones (Veizer, 1983; Fallah-Baghtash et al., 2020).

## GEOCHEMISTRY OF THE CARBONATES

Both the concentrations of some trace elements (strontium, sodium, iron and manganese) and the stable-isotope compositions of the oxygen and carbon in the carbonates have been investigated (Tables 1 and 2) with the objective to get a better insight into the diagenetic processes that affected the sediments.

The recognition of the original carbonate mineralogy of limestones in the sedimentary record based on petrographic studies is difficult: during meteoric and/or burial diagenetic conditions, aragonite and high-magnesium calcite are unstable and metastable carbonate phases, and they will be transformed into low-magnesium calcite and dolomite. These processes thus

## TRACE ELEMENTS

Trace elements in the carbonates become mixed with those from the diagenetic fluids and then are repartitioned during recrystallization, mineral precipitation, and stabilization (Veizer, 1983). The most important of the processes that result in the incorporation of these elements in the limestone is substitution for Ca (Veizer, 1983).

The strontium concentrations in the investigated 48 limestones of the Asmari Formation range from 17 to 1402 ppm, with an average value of 709.5 ppm (Table 1 and Fig. 9A). This is lower than in recent warm-water aragonite carbonates, which tend to show concentrations in the range of roughly

Table 1

**Elemental and isotopic composition of the investigated  
48 limestone and 32 dolomite samples from the Asmari Formation**

Rock type		Mg [%]	Mn [ppm]	Fe [ppm]	Na [ppm]	Sr [ppm]	$\delta^{18}\text{O}_{\text{‰}}$ [V-PDB]	$\delta^{13}\text{C}_{\text{‰}}$ [V-PDB]
limestone	max	3.1	290	10307	4499	1402	-0.85	1.56
	min	0.04	2	28	275	17	-8.96	-5.86
	average	0.9	146	5167	2387	709.5	-2.99	-0.74
D1	max	12.23	100	2702.8	1632.6	347.2	-	-
	min	9.96	33.2	749.7	987.4	55.26	-	-
	average	11.18	50.7	1273.7	1262.5	131.1	-	-
D2	max	11.16	288.7	7872.8	3447	2414.9	-	-
	min	4.01	47.7	1404.2	581.9	45.2	-	-
	average	7.46	136.5	4220.7	1694.8	598.1	-	-
D3	max	10.9	190.3	3616.4	2789.9	1402.3	-	-
	min	4.05	30.6	1019.5	746	107.1	-	-
	average	7.96	94.39	1911	1585.7	448.3	-	-

8,000–10,000 ppm (Milliman, 1974). The strontium concentration of the 32 investigated dolomites ranges from 45 to 757 ppm with a mean value ranging from 131 ppm (D1) to 448 ppm (D3) (Table 1). It is relevant in this context that the strontium content is larger in aragonite than in high-magnesium calcite because  $\text{Sr}^{2+}$  cations are larger than  $\text{Ca}^{2+}$  and therefore preferentially enter into the orthorhombic crystal lattices of aragonite (e.g., Veizer, 1983; Morrison and Brand, 1986). The low levels of strontium in the carbonates under study suggest that the precursor aragonite of the Asmari carbonates was depleted in strontium, which reflects the diagenetic equilibration that followed the exposure of the unstable aragonitic precursor sediment to meteoric water (Brand and Veizer, 1980). The Sr content in aragonite is usually high, while the Mn content is low (Cantrell, 2006). Therefore, the weak negative correlation between Mn and Sr in the studied samples reflects a limited diagenetic equilibration under the meteoric phreatic conditions (Fig. 9A). The relatively high concentration of Sr in the Asmari dolomites may be due to the formation of these dolomites by replacement of carbonates with an original aragonite mineralogy or precipitation of dolomite from saline dolomitizing fluids.

The Na concentrations in the limestones range from 275 to 4499 ppm with an average value of 2387 ppm. The amount of Na in these limestones thus is higher than in recent warm-water aragonitic sediments (2,700 ppm; Milliman, 1974) and their calcitic (270 ppm; Veizer, 1983) counterparts (Fig. 9B). The relatively large amounts of sodium in the Asmari limestones must be ascribed to the high salinity of the depositional setting with warm to temperate shallow water in the hot and arid Oligo-Miocene climate.

The sodium content in the dolomites ranges from 582 to 3447 ppm, with average values ranging from 1262 ppm (D1) to 1663 ppm (D3) (Table 1).

Iron and manganese are dealt with together here because of their similar origin and behaviour in solution, and because of their similar distribution coefficients ( $D > 1$ ) in carbonates (Vincent et al., 2006). In the Asmari limestone samples, the manganese values are between 2 and 290 ppm, with a mean average value of 146 ppm (Table 1 and Fig. 9C, D). In contrast to the relatively small range of the manganese concentrations, the Fe content varies largely, viz. from 28 to 10,307 ppm, with an average value of 5167 ppm (Table 1 and Fig. 9C). These Fe values are significantly higher than in modern aragonite (20–30 ppm),

where the presence of iron is negligible (Veizer, 1983). The high values of Fe in some samples is most probably due to associated minerals such as pyrite and iron oxides. The iron concentration in the dolomites varies from 750 to 7873 ppm with average values ranging from 1273.7 ppm (D1) to 1911 ppm (D3), and the manganese concentration varies between 31 to 289 ppm, with average values ranging from 51 ppm (D1) to 94 ppm (D3) (Table 1).

In addition to the low Mg values, the Asmari limestones have relatively high Sr/Mn values (Fig. 9E).

#### OXYGEN AND CARBON ISOTOPIC COMPOSITION OF THE LIMESTONES

The bulk-rock oxygen and carbon isotopic analyses of the Asmari limestones are presented in Table 2 and Figure 10, where they are compared with similar analyses of the Asmari Formation in the Dezful Embayment (Aqrabi et al., 2006) and of other Paleogene-Neogene carbonates (Veizer et al., 1999). The  $\delta^{18}\text{O}$  values of the Asmari limestones range from -8.96 to -0.85‰ VPDB (mean -2.99‰), whereas the  $\delta^{13}\text{C}$  values range from -5.86 to +1.56‰ (mean -0.74‰). It can be deduced from Figure 10 that the  $\delta^{18}\text{O}$  and  $\delta^{13}\text{C}$  values correlate well with those found by Aqrabi et al. (2006) for the Asmari Formation, but show slightly lower  $\delta^{18}\text{O}$  and  $\delta^{13}\text{C}$  values than those mentioned by Veizer et al. (1999) for the Paleogene-Neogene carbonates.

#### INTERPRETATION OF THE GEOCHEMICAL DATA

The geochemical and isotopic data (Tables 1 and 2) allow, in combination with the petrographic data obtained from X-ray diffractometry, thin-section analysis and SEM images, recognition of the primary aragonite mineralogy and the evolution of the rock fabric, as well as a reconstruction of the diagenetic evolution, which, in turn, may provide insight into the various conditions that influenced the mineralogy of the sediments during deposition and diagenesis. This regards in particular the temperature, the nature of the percolating fluids, and the water/rock ratio.

Table 2

## Elemental and isotopic composition of selected limestone samples

Sample No.	Rock type (mineralogy)	Depth [m]	$\delta^{18}\text{O}_{\text{‰}}$ [V-PDB]	$\delta^{13}\text{C}_{\text{‰}}$ [V-PDB]	Fe [ppm]	Mn [ppm]	Na [ppm]	Sr [ppm]	Z value
S-2	100% calcite	3329.34	-1.18	-2.23	-	-	-	-	122.15
S-4	100% calcite	3322.87	-1.34	0.31	3378	41	2171	589	127.27
S-5	80% calcite, 20% clay	3318.84	-1.12	-0.39	7747	53	2015	507	126
S-5 QCD	80% calcite, 20% clay	3318.84	-1.11	-0.41	-	-	-	-	126
S-6	85% calcite, 15% clay	3315.72	-1.59	-2.46	873	22.2	1459	374	121.5
S-8	80% calcite, 20% dolomite	3311.32	-0.85	-0.65	3210	40	2514	341	125.5
S-9	100% calcite	3303.34	-1.4	0.48	1778	28.2	1402	4098	127.6
S-11	95% calcite, 5% clay	3295.57	-1.71	-0.37	4096	41	1799	380	125.7
S-12	90% calcite, 10% anhydrite	3293.19	-1.73	-0.21	1996	31	730	-	126
S-14	80% calcite, 20% dolomite	3292.19	-1.67	0.2	2340	35	1435	381	126.9
S-16	90% calcite, 10% dolomite	3288.5	-1.74	1.04	2378	46	2790	757	128.6
S-19	85% calcite, 15% dolomite	3280.32	-3.02	0.2	-	-	-	-	126.2
S-22	80% calcite, 20% dolomite	3273.17	-2.49	-0.55	912	31.2	1445	199	125
S-24	85% calcite, 15% dolomite	3264.15	-3.2	-0.66	405.5	42	3202	240	124.4
S-25	100% calcite	3262.51	-4.66	-0.8	411	36	455	121	123.3
S-25 QCD	100% calcite	3262.51	-4.66	-0.81	-	-	-	-	123.3
S-27	100% calcite	3260	-3.5	-1.37	453.5	32	4499	227	122.8
S-28	100% calcite	3257.5	-2.66	-0.82	824	58	2521	234	124.3
S-29	100% calcite	3253.44	-3.41	-0.97	367	40	1348	181	123.6
S-31	100% calcite	3244.5	-5.01	-1.37	832	37.4	899	623	122
S-32	100% calcite	3237.75	-2.78	-0.55	823	50	1947	190	124.8
S-35	100% calcite	3233.08	-2.28	0.28	6410	127	3015	-	126.7
S-36	100% calcite	3231.3	-2.63	0.44	603.3	45	2069	314	126.9
S-39	100% calcite	3222.74	-1.12	0.82	3616	141	2051	158	128.4
S-40	100% calcite	3218.24	-2.22	1.32	770	82	2112	202	128.9
S-42	100% calcite	3214.73	-1.93	1.4	618	104	1900	195	129.2
S-47	100% calcite	3197.74	-1.59	1.56	1275	88	1433	227	129.7
S-49	100% calcite	3193.55	-1.83	0.8	1038	101	931	289	128
S-50	100% calcite	3180.56	-1.87	0.23	2141	146	1556	276	126.8
S-51	Essentially no peaks - 100% quartz?	3180.3	-1.23	0.44	164	2	275	1402	127.6
S-52	100% calcite	3178.22	-2.18	0.1	904	171	779	243	126.4
S-54	50% calcite, 50% quartz	3152.49	-8.21	-5.86	1247	100	531	177	111.2
S-55	90% calcite, 10% quartz	3135.95	-7.97	-4.54	2955	240	544	3342	114
S-56	100% calcite	3133.94	-8.96	-5.41	2405	261	722	349	111.8
S-57	20% calcite, 20% dolomite, 60% quartz	3112.3	-1.27	0.32	5438	154	1336	201	127.3
S-59	98% calcite, 2% anhydrite	3108.83	-5.03	-2.77	2181	290	986	347	119.1
S-59 QCD	98% calcite, 2% anhydrite	3108.83	-5.06	-2.79	-	-	-	-	119
S-62	70% calcite, 15% dolomite, 15% quartz	3090.75	-2.86	0.88	2433	183	1717	401	127.7
S-63	100% calcite	3082.65	-4.2	-2.37	2639.4	111	883	434	120.4
S-65	100% calcite	3070.12	-4.87	-1.59	966	239.2	602	404	121.6
S-68	100% calcite	3052.73	-2.37	-1.12	1645.3	111	627	1073	123.8
S-70	100% calcite	3050	-3.43	-1.58	1384	87	486	247	122.4
S-75	100% calcite	3040.39	-4.4	0.17	385	72	556	1215	125.5
S-77	90% calcite, 10% dolomite	3015.89	-3.36	-1.49	552	84	1066	267	122.6
S-77 QCD	90% calcite, 10% dolomite	3015.89	-3.36	-1.51	-	-	-	-	122.5
S-80	65% calcite, 35% quartz	2999.15	-3	-1.95	750	79.2	1118	247	121.8
S-84	100% calcite	2965.22	-2.89	0.51	412	10.1	654	452	126.9
S-87	100% calcite	2959.19	-2.51	0.48	476	13	620	402	127

PRECURSOR MINERALOGY  
OF THE ASMARI FORMATION

The studied limestones show warm-water characteristics, such as abundant algae, diverse skeletal and non-skeletal grains, evaporites (Fig. 7A) and early diagenetic dolomites (Fig. 7D, E). Also the composition of the carbonates with a high frequency of dissolved originally aragonitic bivalve and gastropod shells (Fig. 8A), selective dolomitization, occurrence of isopachous rim cement (Fig. 6E), shattered micritic envelopes (Fig. 5D) and extensive fabric-selective dissolution of originally aragonitic grains (Fig. 8A) suggests that aragonite was the original carbonate mineral of the formation.

Selective dolomitization of matrix and some particles can be related to the original aragonite mineralogy of the Asmari carbonates (Fig. 6E), because aragonite mineralogy acts as a catalyst and accelerates dolomitization (Adabi and Rao, 1991; Adabi, 2009). Moreover, aragonite is replaced by dolomite with a retentive and/or destructive texture during progressive diagenesis. Acicular and bladed isopachous rim cement in the form of aragonite crystals (now replaced by dolomite) is the dominant marine cement around framework grains of the Asmari microfacies (Fig. 6E); this has also been reported from numerous modern, warm and shallow seas (Sandberg, 1985; Adabi and Rao, 1991; Fallah-Baghtash et al., 2020). Acicular and bladed isopachous rim cement can be best maintained when the water/rock interaction is low and when the diagenetic system is

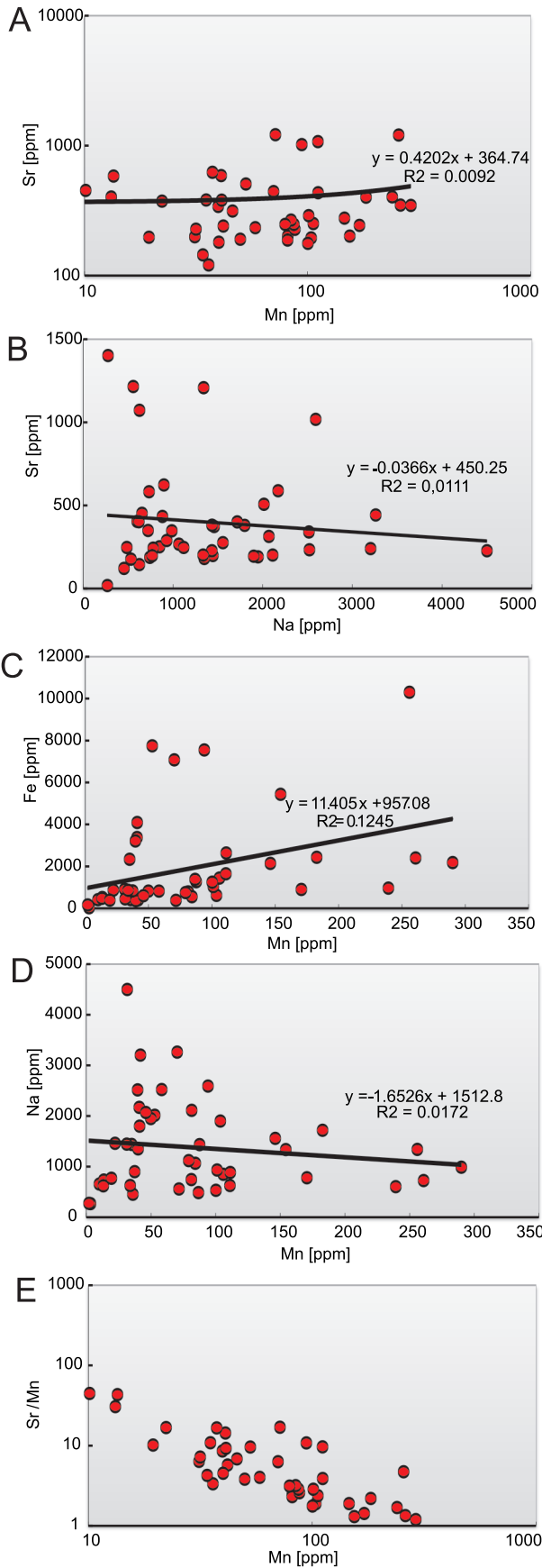


Fig. 9. Relationships between the concentrations of the investigated major elements in the Asmari limestones

closed to semi-closed (Adabi et al., 2008). Shattered micritic envelopes indicate aragonite dissolution during meteoric diagenesis, as observed in both our lagoonal microfacies (Fig. 5D) and elsewhere (Adabi and Rao, 1991).

DIAGENETIC STABILIZATION

Incorporation of trace elements into carbonate minerals is controlled by: (1) the concentration of trace elements in percolating fluids, (2) the water/rock ratio of the diagenetic system, and (3) the distribution coefficient of the trace element for a particular mineral/fluid system (Tucker and Wright, 1990), precursor carbonate mineralogy, temperature, dolomitizing fluids and reduction or oxidation state (Hou et al., 2016; Fallah-Baghtash et al., 2020; Table 1).

The strontium concentration in carbonates is used to study both the precursor mineralogy of ancient limestones and their diagenetic conditions and evolution (Veizer and Demovic, 1973; Veizer, 1983; Winefield et al., 1996; Khatibi-Mehr and Adabi, 2014). The low levels of strontium in the studied limestones indicate that the precursor aragonite was depleted in strontium, which reflects the diagenetic equilibration that proceeded following the exposure of the unstable aragonitic precursor sediment to meteoric water (Brand and Veizer, 1980). The weak negative correlation between Mn and Sr in the studied samples reflects limited diagenetic equilibration in the meteoric phreatic zone (Fig. 9A). The Sr content tends to decrease with increasing water depth and temperature (Morse and MacKenzie, 1990; Cantrell, 2006).

The relatively high concentration of Sr in the dolomites may be ascribed to replacement of carbonates in which the original aragonite was replaced by dolomite under the influence of saline dolomitizing fluids (Azomani et al., 2013; Table 1). Dolomite usually has a lower Sr concentration than calcite due to a lower distribution coefficient of Sr in dolomite, as well as a lower Sr content in dolomitizing fluids (Huang, 2010).

Salinity, biological fractionation, kinetics, mineralogy, and water depth control the concentration of Na in carbonates (Land and Hoops, 1973; Morrison and Brand, 1986). The enriched Na values of the Asmari carbonates may be related to

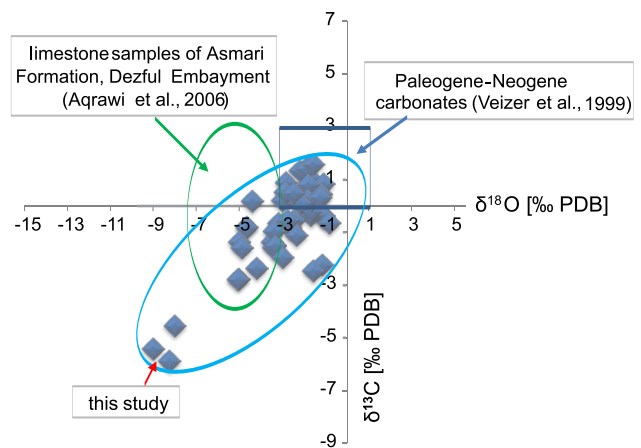


Fig. 10. Comparison of the carbon- and oxygen-isotopic compositions of the Asmari limestones samples in the study area with the Paleogene-Neogene carbonates investigated by Veizer et al. (1999) and the Asmari Formation limestones in the Dezful Embayment investigated by Aqravi et al. (2006)

the high salinity of the depositional environment. Aragonite was the original mineral and reflects a limited diagenetic equilibrium in the meteoric phreatic setting and the presence of iron-bearing clay minerals (cf. Swart, 2015; Fallah-Baghtash et al., 2020). Na and Sr both have a distribution coefficient of  $<1$ , so that their concentration in the meteoric fluids is very low (Adabi and Rao, 1991). The weak correlation between Na and Sr in the samples from the Asmari limestones may be due to high Na concentrations incorporated in aragonite during high-salinity conditions (Fig. 9B).

Iron and manganese with a similar origin show a similar behaviour in solution; this results in similar distribution coefficients ( $D > 1$ ) in carbonates (Vincent et al., 2006). Variations in  $Fe^{2+}$  and  $Mn^{2+}$  concentrations in carbonates, which depend on Eh and pH conditions, are commonly used to trace the diagenetic pathways of carbonates (Tucker and Wright, 1990; Rouxel et al., 2005; Herndon et al., 2018). The poor correlation between Fe and Mn is most probably due to insignificant diagenetic alteration by non-marine fluids during meteoric diagenesis (Fig. 9C) as such diagenesis and reducing conditions increase the amount of these elements in carbonates (Rouxel et al., 2005; Herndon et al., 2018). The positive correlation between iron and manganese values in the Asmari dolomites indicates the alteration of the dolomites by diagenetic fluids in a reducing setting (Fallah-Baghtash et al., 2020). The somewhat negative trend for Mn and Na proves that the low Mn values (Fig. 9D) in the limestone samples of the Asmari Formation can be related to both the composition of the original aragonite minerals and the closed to semi-closed diagenetic system (Fig. 11).

The D3 dolomites (with high concentrations of iron and manganese) were more affected by diagenetic alteration than the D1 dolomites. Due to oxidizing conditions, the iron and manganese values in the (near-surface) S1 dolomites are lower than in the (burial) D3 dolomites which formed under more reducing conditions during deeper burial (cf. Tucker and Wright, 1990; Hou et al., 2016). The very fine- to fine-crystalline dolomites with low iron and manganese contents may consequently have formed during

early diagenesis in an oxidizing setting. Sabkha evaporation of supratidal muddy sediments and seepage reflux through subtidal sediments resulted in the formation of D1 and D2 in carbonate microfacies with different textures (cf. Aqrabi et al., 2006). The higher Fe and Mn content in the coarse-crystalline dolomites (D3) must be ascribed to precipitation in a reducing environment during shallow to relatively deep burial.

#### SOURCES OF THE DIAGENETIC FLUIDS

The relationship between the values of the oxygen and carbon isotopes is a powerful tool for determining the diagenetic evolution, because oxygen and particularly carbon isotopes are very sensitive to diagenetic processes and conditions (Immenhauser et al., 2008; Vincent et al., 2010). The values for the Asmari samples show that these limestones, which have a low content of organic matter, were partially affected by burial diagenesis (Fig. 10). Because of the geothermal gradient, the oxygen isotopes are more affected during burial than the carbon isotopes (Adabi, 2004). The bulk-rock  $\delta^{18}O$  and  $\delta^{13}C$  values of the Asmari limestones and the corresponding values for the limestone samples from the Asmari Formation in the Dezful Embayment (Aqrabi et al., 2006) and for the Paleogene-Neogene carbonates (Veizer et al., 1999) cover fairly comparable values (Fig. 10). This indicates that the stable-isotope composition of the Asmari limestones is fairly original and that this composition was in quite good isotopic equilibrium with the Paleogene seawater. Some samples were affected, however, by later diagenetic processes during burial depth in a closed to semi-closed diagenetic system (see section: WATER/ROCK RATIO and Fig. 11).

It must be concluded from the above that seawater was the main fluid that was involved in the diagenetic modifications of the sediments. This is supported by the Z-value of the sediments, a parameter that is commonly used to distinguish between marine (seawater) and meteoric (rainwater) as the main diagenetic fluid (Keith and Weber, 1964; Zhang et al., 2000; El-Shazly et al., 2011). On this basis, it is possible to differentiate the influence of marine and fresh-water environments in the various parts of the Asmari Formation using this salinity factor.

There is a direct connection between the salinity (Z-value) and the oxygen-isotope composition ( $\delta^{18}O$ ) of the seawater (Epstein and Mayeda, 1953). Evaporation and fresh-water inflow are the two main factors influencing the salinity of seawater. Due to evaporation, salinity and heavy oxygen isotopes increase in saline water. On the other hand, fresh-water runoff and direct precipitation into the ocean have negligible salinity and are depleted in heavy isotopes because of fractionation during initial evaporation in the hydrological cycle (Raisback et al., 1989). In the present study, the salinity index (Z-value) was estimated from the isotopic values (V-PDB) using the following equation proposed by Keith and Weber (1964):

$$Z = 2.048(\delta^{13}C+50) + 0.498(\delta^{18}O+50)$$

Limestones with a Z-value  $>120$  indicate marine conditions, whereas those with a Z-value below 120 represent fresh water, and limestones with a Z-value close to 120 indicate an environment intermediate between fresh and marine (Keith and Weber, 1964). All Asmari samples show mean Z-values  $>130.07$ , i.e., they indicate a dominantly marine depositional and diagenetic environment (Table 2).

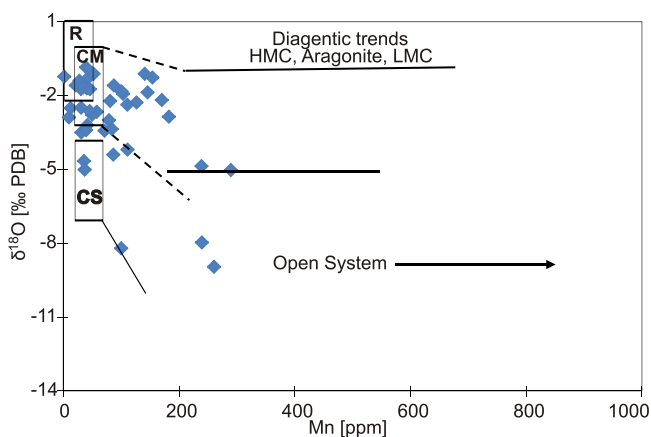


**Fig. 11. Relationship between the  $\delta^{18}O$  value and the Mn content**

The data from the present study are indicated by coloured triangles; the  $\delta^{18}O$  value on the vertical axis is a measure for the degree of rock/water interaction and/or the openness of the system; the Mn content on the horizontal axis is a measure of the redox conditions of the system during precipitation

## SEAWATER TEMPERATURE

The oxygen isotopic composition can be used for determining the temperature of the seawater at the time of deposition (Anderson and Arthur, 1983; Veizer and Mackenzie, 2014; Fallah-Bagtash et al., 2020) as well as its salinity (Keith and Weber, 1964; Madhavaraju et al., 2004; Narayanan et al., 2007). The isotopic composition of the diagenetic fluids (i.e., not evaporitic fluids but, for instance, meteoric fluids) is typically depleted in  $^{18}\text{O}$  relative to coeval marine water except for fluids of evaporitic origin. In general,  $\delta^{18}\text{O}$  values for carbonate minerals decrease with time (Veizer and Hoefs, 1976). Veizer (1983) explained this by diagenetic modification of the carbonates by  $\delta^{18}\text{O}$ -depleted meteoric water, changes in  $\delta^{18}\text{O}$  and  $\delta^{13}\text{C}$  of the seawater; and increase in seawater temperature.

The range of the  $\delta^{18}\text{O}$  values in the samples from the Asmari Formation indicates a sedimentary temperature from 23 to 68.8°C (average 33°C) following the equation of Anderson and Arthur (1983):

$$T = 16 - 4.14 (\delta\text{c} - \delta\text{w}) + 0.13 (\delta\text{c} - \delta\text{w})^2$$

where:  $T$  is the seawater temperature (in °C),  $\delta\text{c}$  is the oxygen-isotope value in the limestone samples, and  $\delta\text{w}$  is the oxygen-isotope value of Paleogene marine water, i.e., 0.8‰ SMOW (Standard Mean Ocean Water), as measured by Veizer et al. (1999).

The input of the Asmari values in the Anderson and Arthur (1983) formula gives a remarkable result: one of the  $\delta^{18}\text{O}$ -depleted samples (−8.96‰) yields a temperature of 68.8°C, which must, obviously, represent a temperature during burial diagenesis. One of the  $\delta^{18}\text{O}$ -enriched samples (−0.85‰) gives a syn-sedimentary temperature of only 23°C. This latter temperature is consistent with the presence of the fauna, including large benthic foraminifers, corals, and red algae, and also with the non-biogenic contents such as peloids and ooids. It also is a reasonable outcome considering the latitude of the Zagros sedimentary basin during the Oligo-Miocene (30°N) (Heydari, 2008).

## WATER/ROCK RATIO

The diagenetic trends for low-magnesium calcite (LMC), high-magnesium calcite (HMC), aragonite (A) in recent sediments (R), the Mississippian Burlington Limestone in Mississippi (CM), and the Silurian Read Bay Limestone in Alabama (CS) are shown by rectangles in Figure 11, based on Milliman (1974) and Brand and Veizer (1980). Their diagenetic trends are indicated by the drawn and dashed lines. This shows the type of diagenetic system (open or closed), the water/rock ratio or interaction, and the oxidation/reduction conditions of the depositional carbonate system involved. Most limestone samples of the Asmari Formation (which are shown by blue diamonds in Fig. 11) are found to be positioned within the field of recent sediments (R) and the Burlington Limestone (CM), which have undergone little alteration and indicate a low water/rock interaction in a closed to semi-closed diagenetic system. A low Mn concentration in a diagenetic stage is an indicator of a closed diagenetic system (Brand and Veizer, 1980; Fig. 11). Repeated alternations of dissolution and precipitation prevent diagenetic fluids to leave the diagenetic system. Consequently, there is little water/rock interaction in a closed diagenetic system, even though the diagenetic fluids may change constantly (Knorich and Mutti, 2006). It is therefore the distribu-

tion coefficient that controls the relative enrichment or depletion of the major and trace elements in the diagenetic fluid (Knorich and Mutti, 2006; Caron and Nelson, 2009).

Plotting the Sr/Mn ratio versus Mn helps estimating the dissolution rate of limestones (Rao, 1991). The relatively high Sr/Mn values (Fig. 9E) indicate a closed to semi-closed diagenetic system for the carbonates of the Asmari Formation. Samples with a high Mn content have been exposed to relatively long-lasting diagenetic alteration by meteoric water and thus have undergone the strongest dissolution (Fig. 9E).

## DIAGENETIC EVOLUTION

The Asmari Formation has undergone a complex diagenetic evolution, from penecontemporaneous shallow-marine consolidation to deep-burial diagenesis (Fig. 12). The various stages that can be distinguished are marine diagenesis (early diagenesis), meteoric diagenesis (middle diagenesis), and shallow and deep burial diagenesis (late diagenesis).

### MARINE DIAGENESIS

In the syndepositional diagenetic stage, the Asmari Formation developed along a homoclinal ramp-type carbonate platform. The limestones were deposited as mudstones, wackestones, packstones, grainstones, rudstones, and floatstones. The diagenetic processes that occurred during and shortly after deposition are micritization of grains, bioturbation, and precipitation of acicular rim aragonite, bladed isopachous rims, peloidal micrite, and rarely marine vadose meniscus calcite cement.

Micritization and bioturbation commonly occur in relatively low-energy shallow-marine environments and indicate intense microbial activity (Flügel, 2010). These two early-diagenetic processes hardly affected the reservoir quality.

Acicular and bladed isopachous rim cement types are characterized by fairly thin layers lining intra- and intergranular pores in grainstones and rudstones (Fig. 6E). These early-diagenetic cements were later covered by calcite cement during late diagenesis (Fig. 6I). Scoffin (1987) placed these cement types in the group of marine cements. Meniscus or crescent cements (Fig. 6F) are essentially formed in the marine vadose zone (James and Choquette, 1990; Tucker and Wright, 1990). The micritic fabric of this cement and possibly its high-magnesium calcite mineralogy are characteristic of a marine vadose setting.

The anhydrite (or former gypsum) crystals in the form of nodular, layered, sparse, and isolated anhydrite crystals precipitated within fenestral and pore spaces in micrite and dolomicrite of a supratidal/sabkha environment (Fig. 7B). The anhydrite originated from supersaturated brines and by evaporation in the hot and arid climate.

The high-Mg calcitic matrix was preferentially dolomitized by slightly modified seawater (in the sabkha), producing very fine- to fine-crystalline dolomite in the muds (Fig. 7D). Replacement of dolomite before the onset of chemical compaction is shown by the early low-amplitude stylolites that cross-cut the dolomite (Fig. 6B), the very fine-crystalline texture, the high Sr and low Fe and Mn content (Table 1), the well-preserved precursor-limestone texture (Fig. 7D; Aqrabi et al., 2006) and the presence of nodular anhydrite and sparse evaporite crystals (Fig. 7B). Rahimpour-Bonab et al. (2010) suggest that the very fine- to fine-crystalline dolomite formed during a very early diagenetic stage in an oxidizing setting.

Diagenetic Events		Diagenetic Sages				
Process	Features	Marine	Meteoric	Shallow Burial	Deep Burial	
<b>Biologic</b>	Microbial micritization	=====				
	Accretionary micritic envelopes	=====				
	Bioturbation	=====				
	Boring	=====				
	Burrow	=====				
<b>Dissolution</b>	Fabric selective		=====	-----	=====	
	Fabric destructive		-----	-----	=====	
	Karstification		=====			
<b>Cementation</b>	Acicular isopachous rim	=====				
	Bladed isopachous rim cement	=====				
	Peloidal micrite cement	=====				
	Meniscus cement	=====	-----			
	Equant calcite cement		=====	-----	-----	
	Drusy calcite cement		=====	-----	-----	
	Syntaxial overgrowth cement		=====	=====	=====	
	Poikilotopic calcite cement			=====	=====	
Coarse sparry calcite cement			=====	=====		
<b>Neomorphism</b>	Recrystalization of Ar and HMC to LMC		=====	-----		
	Microspar		=====	-----		
	Pseudospar		=====	-----	-----	
<b>Compaction</b>	<b>Mechanical</b>	Closer grain packing			=====	
		Reorientation			=====	
		Ductile deformation			=====	
		Compaction of algal mat			=====	
		Broken allochem			=====	
		Broken micrite envelopes			=====	
		Compression of peloids			=====	
		Fracturing				=====
	<b>Chemical</b>	Convex-concave contact				=====
		Sutured contact				=====
		Solution seams				=====
		Stylolite				=====
<b>Dolomitization</b>	Sabkha dolomite (dolomicrite)	=====				
	Mixed meteoric-marine dolomite		=====			
	Seepage-reflux dolomite			=====		
	Burial dolomite			-----	=====	
	Saddle dolomite			-----	=====	
	Bacterial mediation dolomite			-----	=====	
	Fe dolomite			-----	=====	
Neomorphic dolomite			-----	=====		
<b>Anhydritization</b>	Sparse anhydrite crystal	=====				
	Anhydrite nodules	=====		-----	=====	
	Replacment anhydrite		=====	=====	=====	
	Vein-filling anhydrite			-----	=====	
	Poikilotopic anhydrite			=====	=====	
	Pervasive anhydrite				=====	
	Fracture-filling anhydrite				=====	
Stylolite-filling anhydrite				=====		
<b>Pyritization</b>	Framboidal pyrite	=====				
	Cubic pyrite				=====	
<b>Silicification</b>					=====	
<b>Glauconite</b>					=====	

Fig. 12. Overview of the diagenetic evolution of the Asmari Formation

### METEORIC DIAGENESIS

The diagenetic processes that affected the Asmari carbonates during this stage were precipitation of syntaxial, equant, and drusy calcite cement by mixed meteoric/marine fluids, neomorphism, fabric-selective dissolution, and dolomitization. Dolomite forming in a mixing zone has several distinct characteristics, including high Mn concentrations (Table 1), and inclusion-free crystals <100 µm in size.

Equant and drusy calcite cement commonly filled mouldic pore spaces that had resulted from the fabric-selective dissolution of skeletal components such as bivalves, gastropods, and some foraminifers (Fig. 6H, I); these cement types also filled intergranular pores where these had not been filled by a mud matrix.

James and Choquette (1990) and Tucker and Wright (1990) suggested that these cements are formed under both meteoric and burial diagenetic conditions. A meteoric origin of these cement types seems the most likely for the Asmari Formation, because of overgrowths on first-generation (marine) cement and the fine crystal size. Syntaxial cement is widespread in sediments with echinoderm debris. Since the syntaxial cement in the Asmari Formation does not contain inclusions and has a clear appearance (Fig. 6G), its formation should be attributed to a meteoric phreatic setting (cf. Tucker and Wright, 1990; Tucker, 2001).

### SHALLOW-BURIAL DIAGENESIS

In the shallow-burial setting, with a gradually increasing burial temperature, the carbonate sediments that had not previously been dolomitized during early diagenesis, became all dolomitized. Those that had previously already been dolomitized only experienced recrystallization, as can be deduced from the thin-sections (Fig. 7H). Extensive fabric-preserving dolomitization (Fig. 6E), a well-preserved precursor limestone texture (Fig. 7D; Tucker and Wright, 1990; Machel, 2004), and the significant thickness of the dolomites are evidence of reflux dolomitization in the upper and middle parts of the Asmari Formation (cf. Hou et al., 2016; Jafari et al., 2020). The high Na concentrations support this interpretation (Table 1).

The mechanical compaction (with re-orientation of grains, denser packing, and breaking of allochems) and the precipitation of some equant and drusy calcite cement are characteristic of a shallow-burial setting. Chemical compaction also took place in the form of the genesis of low-amplitude stylolites.

### DEEP-BURIAL DIAGENESIS

There is no clear boundary between the shallow-burial and the intermediate-to-deep-burial stage, because temperature and pressure increase gradually with depth (Machel, 2004). Petrographically, late diagenesis is characterized by coarse poikilopic sparry calcite (Fig. 6J), by pervasive and poikilopic anhydrite cement with large crystals that occludes fractures, vugs and veins (Figs. 5H, I and 6E), due to the infiltration of calcium-sulphate-bearing solutions that resulted from the migration of brines from the Gachsaran Formation into the porous, permeable Asmari Formation. Fabric-destructive dissolution (Fig. 8C), authigenic cubic pyrite and high-amplitude stylolites (Fig. 6C) that cross-cut coarse crystalline dolomites (D3 type, with a high

iron and manganese content) are common. The elevated Mn and Fe levels (which might reflect a reducing environment: Adabi, 2009; Table 1) and the low concentrations of Sr and Na (Table 2) indicate precipitation in a reducing environment.

The formation of some coarse-crystalline dolomites indicates that renewed compaction created new fractures that formed conduits for ascending hydrothermal basement-derived fluids from which saddle dolomite precipitated. The occurrence of saddle dolomite as cement (see section: CEMENTATION), along the edges of vugs, veins, stylolites, and fractures (Fig. 7I) also suggests deep burial. Erosion of the top of the rock column eventually led to a reduced burial depth of the succession and resulted in a last generation of fractures and stylolites. Blocky calcite and sulphides are present along these fractures.

### DIAGENETIC CONTROL OF THE RESERVOIR QUALITY

The primary reservoir potential of sedimentary successions depends on their textural characteristics and depositional setting. The final reservoir quality is determined, however, by post-depositional changes, known as diagenesis and (diagenetic or tectonic) fracturing (Ahr, 2008; Moore and Wade, 2013). This poses a problem for hydrocarbon exploration because the spatial distribution of the various diagenetic features is heterogeneous across any studied sedimentary unit, which implies that significant local differences in porosity and permeability occur. Meteoric and shallow-burial diagenesis tends to enhance the reservoir quality, whereas burial processes (e.g., fabric-destructive dolomitization) tend to decrease both the porosity and the permeability of the targeted potential reservoir. Burial dissolution (in this case: dissolution of anhydrite cement), however, is commonly exceptionally effective in enhancement of a reservoirs' porosity and permeability, and this is the case, indeed, for the Asmari limestones.

Dissolution and fracturing were the main constructive processes for the sediments under study. Meteoric dissolution has significantly increased the porosity by the formation of vuggy and mouldic pores in the uppermost and middle parts of the Asmari Formation. Meteoric dissolution affected particularly the high-energy shoal and lagoonal sediments that developed on the inner ramp.

In contrast, cementation and both mechanical and chemical compaction are the main destructive processes that reduced the reservoir quality. Petrographic analysis indicates that different types of anhydrite and calcite cement have reduced the reservoir quality of the lagoonal and shoal sediments by occluding intergranular and mouldic pores as well as pore throats. Compaction caused a considerable reduction of the rock volume and thus also reduced the reservoir quality. Stylolites tend to reduce porosity locally to the degree that dissolved carbonate becomes re-precipitated rather than transported. Recent studies (e.g., Heap et al., 2014) indicate, however, that stylolites and other solution seams, as common products of chemical compaction, can also act as flow paths, especially along their strike in a horizontal direction.

Dolomitization had both positive and negative effects on the reservoir quality. It improved the reservoir quality by widening intercrystalline pores that are interconnected (Fig. 7F, G). On the other hand, extensive dolomitization has reduced the reservoir quality by creating a dense, interlocking fabric (Fig. 7H).

Micritization and bioturbation had no distinct major influence on the reservoir quality of the Asmari carbonates, although it cannot be fully excluded that their role is not yet well-understood. Micritization created micropores that may have facilitated porosity preservation because of the so-called "pore-size-controlled solubility" phenomenon (Ehrenberg and Walderhaug, 2015). Considering that the accretionary micritic envelopes occur mainly in the lower part of the Asmari Formation where mud-supported sediments prevail, it is unlikely that the accretionary micritic envelopes affected the porosity here.

Bioturbation, which itself did not affect the reservoir quality, created suitable conditions in the reservoir for the development of diagenetic processes such as cementation, dissolution, and dolomitization, that affected the reservoir quality, as shown by several previous studies (e.g., Taghavi et al., 2006; Hollis, 2011).

## DISCUSSION

Because the Oligocene-Miocene Asmari Formation is located in a region where hydrocarbons have been found, the carbonates of this formation are a potential target for exploration activities. Efficient exploration requires insight into not only the tectonic structure (which is relatively simple here), but particularly in the characteristics of the limestones and their vertical and lateral variations. This implies that the sedimentological setting and the diagenetic alterations of the limestones must be known in detail.

Because the sediments can be studied only in a limited number of sections, the precise lateral and vertical microfacies distribution requires interpretation, mainly on the basis of thin-section analysis of core samples. Numerous earlier studies have proposed how microfacies should be distinguished, and what more or less precise depositional conditions they represent. These insights are based also on comparison with recent settings, although such a comparison is hampered by the scarcity of modern marine carbonate environments. Yet, it is commonly accepted that microfacies interpretation of carbonates as presented by, among others, Flügel (2010) is a valuable tool.

Consequently, we have followed such an approach, and this resulted in the recognition of a large number of microfacies, which appeared distributed in such a way that a logical model of the study area during deposition of the Asmari Formation could be established (Fig. 4). It should therefore be considered a feasible set of data for future exploration activities.

Regarding the potential hydrocarbon occurrences it should be realized, however, that not only have several diagenetic processes increased the reservoir quality of the Asmari Formation, but that other diagenetic processes have reduced the quality,

particularly by reducing the porosity and permeability of the limestones. The net effect of these mutually contrasting developments still needs further investigation.

## CONCLUSIONS

Sedimentological evaluation of the Asmari Formation in the Shadegan Oil Field has resulted in the following general conclusions.

The Asmari carbonates were deposited on an extensive homoclinal ramp-type carbonate platform and partly in an open-marine setting.

Differences in grain properties, texture, inferred water depth, and energy level make it possible to distinguish 26 carbonate microfacies on the basis of thin-section analysis. These microfacies can be grouped into 12 microfacies associations that represent four main environments in an overall shallowing-upward setting from very low-energy open-marine to outer ramp in the lower part of the formation, to a low-energy inner ramp, to a moderate-energy middle part, and eventually to a high-energy upper part. There is evidence of subaerial exposure and evaporitic conditions in the middle and upper parts of the formation.

The bulk-rock  $\delta^{18}\text{O}$  and  $\delta^{13}\text{C}$  values of the Asmari limestones, the low Mn concentration, and the high Sr/Mn values indicate that the stable-isotope composition represent deposition-related features that were hardly changed by diagenetic processes. The composition is in fairly good isotopic equilibrium with the Paleogene seawater, although some samples were affected by later diagenetic processes during burial in a closed to semi-closed diagenetic system with low water/rock interaction.

Diagenetic features changed many other primary properties of the Asmari limestones, which constitute potential targets for hydrocarbon exploration. The main diagenetic features that improved the reservoir quality are dissolution, dolomitization, and fracturing. Occlusion of pores and pore throats as a result of various calcite and anhydrite cementation processes, and of mechanical and chemical compaction decreased the reservoir quality.

Diagenetic processes such as micritization and bioturbation had no distinct influence on the reservoir quality of the Asmari carbonates.

**Acknowledgements.** We acknowledge the NISOC (National Iranian South Oil Company) and the Ferdowsi University of Mashhad, Iran, for providing generous support with supplies for the present contribution (Research code: 3/28564). We thank the three reviewers of our manuscript for their positive-critical comments and suggestions, which greatly contributed to improvements.

## REFERENCES

- Adabi, M.H., 2004. A re-evaluation of aragonite versus calcite seas. *Carbonates and Evaporites*, **19**: 133–141.
- Adabi, M.H., 2009. Multistage dolomitization of Upper Jurassic Mozduran Formation, Kopet-Dagh Basin, N.E. Iran. *Carbonates and Evaporites*, **24**: 16–32.
- Adabi, M.H., Mehmandosti, E.A., 2008. Microfacies and geochemistry of the Ilam Formation in the Tang-E Rashid area, Izeh, SW Iran. *Journal of Asian Earth Sciences*, **33**: 267–277.
- Adabi, M.H., Rao, C.P., 1991. Petrographic and geochemical evidence for original aragonitic mineralogy of Upper Jurassic carbonate (Mozduran Formation), Sarakhs area, Iran. *Sedimentary Geology*, **72**: 253–267.
- Adabi, M.H., Zohdi, A., Ghabeishavi, A., Amiri-Bakhtiyar, H., 2008. Applications of nummulitids and other larger benthic foraminifera in depositional environment and sequence stratigraphy: an example from the Eocene deposits in Zagros Basin, SW Iran. *Facies*, **54**: 499–512.

- Ahr, W.M., 2008. Geology of Carbonate Reservoirs: the Identification, Description, and Characterization of Hydrocarbon Reservoirs in Carbonate Rocks. John Wiley and Sons.
- Alavi, M., 2004. Regional stratigraphy of the Zagros Fold-Thrust Belt of Iran and its proforeland evolution. *American Journal of Science*, **304**: 1–20.
- Amao, A.O., Kaminski, M.A., Setoyama, E., 2016. Diversity of foraminifera in a shallow restricted lagoon in Bahrain. *Micro-paleontology*, **62**: 197–211.
- Anderson, T.F., Arthur, M.A., 1983. Stable isotopes of oxygen and carbon and their application to sedimentologic and paleo-environmental problems. *SEPM Short Course*, **10**: 1.1–1.151.
- Aqrabi, A.A.M., Keramati, M., Ehrenberg, S.N., Pickard, N., Moallemi, A., Svånå, T., Darke, G., Dickson, J.A.D., Oxtoby, N.H., 2006. The origin of dolomite in the Asmari Formation (Oligocene-lower Miocene), Dezful Embayment, SW Iran. *Journal of Petroleum Geology*, **29**: 381–402.
- Asprion, U., Westphal, H., Nieman, M., Pomar, L., 2009. Extrapolation of depositional geometries of the Menorcan Miocene carbonate ramp with ground-penetrating radar. *Facies*, **55**: 37–46.
- Avarjani, S., Mahboubi, A., Moussavi-Harami, R., Amiri-Bakhtiar, H., Brenner, R.L., 2015. Facies, depositional sequences, and biostratigraphy of the Oligo-Miocene Asmari Formation in Marun oilfield, North Dezful Embayment, Zagros Basin, SW Iran. *Palaeoworld*, **24**: 336–358.
- Azomani, E., Azmy, K., Blamey, N., Brand, U., Al-Aasm, I., 2013. Origin of Lower Ordovician dolomites in eastern Laurentia: controls on porosity and implications from geochemistry. *Marine and Petroleum Geology*, **40**: 99–114.
- Bádenas, B., Aurell, M., 2001. Proximal-distal facies relationships and sedimentary processes in a storm dominated carbonate ramp (Kimmeridgian, northwest of the Iberian Ranges, Spain). *Sedimentary Geology*, **139**: 319–340.
- Bordenave, M.L., Hegre, J.A., 2010. Current distribution of oil and gas fields in the Zagros Fold Belt of Iran and contiguous offshore as the result of the petroleum systems. *Geological Society Special Publications*, **330**: 291–353.
- Brand, U., Veizer, J., 1980. Chemical diagenesis of multicomponent carbonate system, II: stable isotopes. *Journal of Sedimentary Petrology*, **51**: 987–997.
- Brigaud, B., Durlet, C., Deconinck, J.F., Vincent, B., Pucéat, E., Thierry, J., Trouiller, A., 2009. Facies and climate/environmental changes recorded on a carbonate ramp: a sedimentological and geochemical approach on Middle Jurassic carbonates (Paris Basin, France). *Sedimentary Geology*, **222**: 181–206.
- Cantrell, D.L., 2006. Cortical fabrics of Upper Jurassic ooid, Arab Formation, Saudi Arabia: implication for original carbonate mineralogy. *Sedimentary Geology*, **186**: 157–170.
- Caron, V., Nelson, C., 2009. Diversity of neomorphic fabrics in New Zealand Plio-Pleistocene cool-water limestones: insights into aragonite alteration pathways and controls. *Journal of Sedimentary Research*, **79**: 226–246.
- Corda, L., Brandano, M., 2003. Aphotic zone carbonate production on a Miocene ramp, Central Apennines, Italy. *Sedimentary Geology*, **161**: 55–70.
- Crowe, S.A., Drssing, L.N., Beukes, N.J., Bau, M., Kruger, S.J., Frei, R., Canfield, D.E., 2013. Atmospheric oxygenation three billion years ago. *Nature*, **501**: 535–538.
- Dickson, J., 1965. Carbonate identification and genesis as revealed by staining. *Journal of Sedimentary Research*, **36**: 491–505.
- Dunham, R., 1962. Classification of carbonate rocks according to depositional texture. *AAPG Memoir*, **1**: 108–121.
- Ehrenberg, S.N., Walderhaug, O., 2015. Preferential calcite cementation of macropores in microporous limestones. *Journal of Sedimentary Research*, **85**: 780–793.
- El-Shazly, S., Košťák, M., Abdel-Gawad, G., Klouk ová, B., Sauer, S.G., Salama, Y.F., Mazuch, M., Žák, K., 2011. Carbon and oxygen stable isotopes of selected Cenomanian and Turonian rudists from Egypt and Czech Republic, and a note on changes in rudist diversity. *Bulletin of Geosciences*, **86**: 209–226.
- Embry, A.F., Klovan, J.E., 1971. A late Devonian reef tract on north-eastern Banks Island, NWT. *Bulletin of Canadian Petroleum Geology*, **19**: 730–781.
- Epstein, S., Mayeda, T., 1953. Variation of O<sup>18</sup> content of waters from natural sources. *Geochimica et Cosmochimica Acta*, **4**: 213–224.
- Fallah-Baghtash, R., Jafarian, A., Husinec, A., Adabi, M.H., 2020. Diagenetic stabilization of the Upper Permian Dalan Formation, Persian Gulf Basin. *Journal of Asian Earth Sciences*, **189**: 104–144.
- Flügel, E., 2010. *Microfacies of Carbonate Rocks: Analysis, Interpretation, and Application*. Springer-Verlag, Berlin.
- Geel, T., 2000. Recognition of stratigraphic sequences in carbonate platform and slope deposits: empirical models based on microfacies analysis of Paleogene deposits in southeastern Spain. *Palaeogeography, Palaeoclimatology, Palaeoecology*, **155**: 211–238.
- Ghazban, F., 2007. *Petroleum Geology of the Persian Gulf*. Tehran University and National Uranian Oil Company Publications, Tehran.
- Gonera, M., 2012. Palaeoecology of the Middle Miocene foraminifera of the Nowy S cz Basin (Polish Outer Carpathians). *Geological Quarterly*, **56** (1): 107–116.
- Heap, M.J., Baud, P., Reuschlé, T., Meredith, P.G., 2014. Stylolites in limestones: Barriers to fluid flow? *Geology*, **42**: 51–54.
- Herndon, E.M., Havig, J.R., Singer, D.M., McCormick, M.L., Kump, L.R., 2018. Manganese and iron geochemistry in sediments underlying the redox-stratified Fayetteville Green Lake. *Geochimica et Cosmochimica Acta*, **231**: 50–63.
- Heydari, E., 2008. Tectonics versus eustatic control on super sequences of the Zagros Mountains of Iran. *Tectonophysics*, **451**: 56–70.
- Hollis, C., 2011. Diagenetic controls on reservoir properties of carbonate successions within the Albian–Turonian of the Arabian Plate. *Petroleum Geoscience*, **17**: 223–241.
- Hood, A., Planavsky, N.J., Wallace, M.W., Wang, X., 2018. The effects of diagenesis on geochemical paleoredox proxies in sedimentary carbonates. *Geochimica et Cosmochimica Acta*, **232**: 265–287.
- Hou, Y., Azmy, K., Berra, F., Jadoul, F., Blamey, N.J., Gleeson, S.A., Brand, U., 2016. Origin of the Breno and Esino dolomites in the western Southern Alps (Italy): implications for a volcanic influence. *Marine and Petroleum Geology*, **69**: 38–52.
- Huang, S.J., 2010. *Carbonate Diagenesis*. Geological Publishing House: 29–44.
- Immenhauser, A., Kenter, J.A., Ganssen, G., Bahamonde, J.R., Van Vliet, A., Saher, M.H., 2002. Origin and significance of isotope shifts in Pennsylvanian carbonates (Asturias, NW Spain). *Journal of Sedimentary Research*, **72**: 82–94.
- Immenhauser, A., Holmden, C., Patterson, W.P., 2008. Interpreting the carbon isotope record of ancient shallow epeiric sea: Lessons from the recent. *Geological Association of Canada Special Publication*, **48**: 135–174.
- Jafari, J., Mahboubi, A., Moussavi-Harami, R., Al-Aasm, I.S., 2020. The effects of diagenesis on the petrophysical and geochemical attributes of the Asmari Formation, Marun oil field, southwest Iran. *Petroleum Science*, **17**: 1–25.
- James, N.P., Choquette, P.W., 1990. Limestones – the meteoric diagenetic environment. *Diagenesis. Geoscience Canada Reprint Series*, **4**: 35–73.
- Keith, M., Weber, J., 1964. Carbon and oxygen isotope composition of selected limestone and fossils. *Geochimica et Cosmochimica Acta*, **28**: 1787–1816.
- Khatibi-Mehr, M., Adabi, M.H., 2014. Microfacies and geochemical evidence for original aragonite mineralogy of a foraminifera-dominated carbonate ramp system in the late Paleocene to Middle Eocene, Alborz Basin, Iran. *Carbonates and Evaporites*, **29**: 155–175.
- Knorrich, A.C., Mutti, M., 2006. Missing aragonitic biota and the diagenetic evolution of heterozoan carbonates: a case study from the Oligo-Miocene of the central Mediterranean. *Journal of Sedimentary Research*, **76**: 871–888.
- Land, L.S., Hoops, G.K., 1973. Sodium in carbonate sediments and rocks: a possible index to salinity of diagenetic solution. *Journal of Sedimentary Petrology*, **43**: 614–617.

- Lashgari, A., Hayhat, M.R., Vergés, J., Beamud, E., Najafi, M., Khatib, M.M., Karimnejad, H.R., 2020. Age of synorogenic deposits and timing of folding in Dezful embayment, SW Zagros Fold Belt. *Marine and Petroleum Geology*, **113**: 104148.
- Lear, C.H., Elderfield, H., Wilson, P.A., 2000. Cenozoic deep-sea temperatures and global ice volumes from Mg/Ca in benthic foraminiferal calcite. *Science*, **287**: 269–272.
- Machel, H.G., 2004. Concepts and models of dolomitization: a critical reappraisal. *Geological Society Special Publications*, **235**: 7–63.
- Madhavaraju, J., Kolosov, I., Buhlak, D., Armstrong-Altrin, J.S., Ramasamy, S., Mohan, S.P., 2004. Carbon and oxygen isotopic signature in Albian–Danian limestones of Cauvery Basin, southeastern India. *Gondwana Research*, **7**: 519–529.
- Milliman, J.D., 1974. *Marine Carbonates Recent Sedimentary Carbonates*, Part 1. Springer, Berlin.
- Moore, C.H., Wade, W.J., 2013. Carbonate reservoirs: porosity, evolution and diagenesis in a sequence stratigraphic framework: porosity evolution and diagenesis in a sequence stratigraphic framework. *Developments in Sedimentology*, **55**.
- Morrison, J.O., Brand, U., 1986. Geochemistry of Recent marine invertebrates. *Geoscience Canada*, **13**: 237–254.
- Morse, J.W., Mackenzie, F.T., 1990. Geochemistry of sedimentary carbonates. *Development in Sedimentology*, **48**.
- Narayanan, V., Anirudhan, S., Grotoli, A.G., 2007. Oxygen and carbon isotope analysis of a Miocene limestone of Kerala and its implications to palaeoclimate and its depositional setting. *Current Science*, **93**: 1155–1159.
- Navabpour, P., Barrier, E., 2012. Stress states in the Zagros fold-and-thrust belt from passive margin to collisional tectonic setting. *Tectonophysics*, **581**: 76–83.
- Omidpour, A., Moussavi-Harami, R., Mahboubi, A., Rahimpour-Bonab, H., 2021. Application of stable isotopes, trace elements and spectral gamma-ray log in resolving high-frequency stratigraphic sequences of a mixed carbonate-siliciclastic reservoirs. *Marine and Petroleum Geology*, **125**: 104854.
- Rahimpour-Bonab, H., Esrafilizadeh, B., Tavakoli, V., 2010. Dolomitization and anhydrite precipitation in Permo Triassic carbonates at the South Pars gas field, offshore Iran: controls on reservoir quality. *Journal of Petroleum Geology*, **3**: 43–66.
- Railsback, L.B., Anderson, T.F., Ackerly, S.C., Cisne, J.L., 1989. Paleooceanographic modeling of temperature salinity profiles from stable isotopic data. *Paleoceanography*, **4**: 585–591.
- Rao, C.P., 1991. Geochemical differences between subtropical (Ordovician), temperate (Recent and Pleistocene) and subpolar (Permian) carbonates, Tasmania, Australia. *Carbonates and Evaporites*, **10**: 114–123.
- Rao, C.P., 1996. *Modern Carbonates, Tropical, Temperate, Polar: Introduction to Sedimentology and Geochemistry*. Hobart: University of Tasmania.
- Rouxel, O.J., Bekker, A., Edwards, K.J., 2005. Iron isotope constraints on the Archean and Paleoproterozoic ocean redox state. *Science*, **307**: 1088–1091.
- Rowlands, G., Purkis, S., Bruckner, A., 2014. Diversity in the geomorphology of shallow-water carbonate depositional systems in the Saudi Arabian Red Sea. *Geomorphology*, **222**: 3–13.
- Sandberg, P., 1985. Aragonite cements and their occurrence in ancient limestones. *SEPM Special Publication*, **36**: 33–57.
- Saura, E., Vergés, J., Homke, S., Blanc, E., Serra-Kiel, J., Bernaola, G., Casciello, E., Fernández, N., Romaine, I., Casini, G., Embry, J.C., 2011. Basin architecture and growth folding of the NW Zagros early foreland basin during the Late Cretaceous and early Tertiary. *Journal of the Geological Society*, **168**: 235–250.
- Saura, E., Garcia Castellanos, D., Casciello, E., Parravano, V., Urruela, A., Vergés, J., 2015. Modeling the flexural evolution of the Amiran and Mesopotamian foreland basins of NW Zagros (Iran Iraq). *Tectonics*, **34**: 377–395.
- Scoffin, T.P., 1987. *An Introduction to Carbonate Sediments and Rocks*. Blackie, Glasgow.
- Sepehr, M., Cosgrove, J.W., 2004. Structural framework of the Zagros fold-thrust belt, Iran. *Marine and Petroleum Geology*, **21**: 829–843.
- Sharland, P.R., Casey, D.M., Davies, R.B., Simmons, M.D., Sutcliffe, O.E., 2004. Arabian plate sequence stratigraphy – revisions to SP2. *GeoArabia*, **9**: 199–214.
- Sherkati, S., Letouzey, J., 2004. Variation of structural style and basin evolution in the central Zagros (Izeh zone and Dezful Embayment), Iran. *Marine and Petroleum Geology*, **21**: 35–55.
- Sherkati, S., Letouzey, J., Frizon de Lamotte, D., 2006. Central Zagros fold thrust belt (Iran): new insights from seismic data, field observation, and sandbox modeling. *Tectonics*, **25**: TC 4007.
- Sibley, D.F., Gregg, J.M., 1987. Classification of dolomite rock textures. *Journal of Sedimentary Research*, **57**: 967–975.
- Sim, M.S., Lee, Y.I., 2006. Sequence stratigraphy of the Middle Cambrian Daegi Formation (Korea) and its bearing on the regional stratigraphic correlation. *Sedimentary Geology*, **191**: 151–169.
- Swart, P.K., 2015. The geochemistry of carbonate diagenesis: the past, present and future. *Sedimentology*, **62**: 1233–1304.
- Taghavi, A.A., Mørk, A., Emadi, M.A., 2006. Sequence stratigraphically controlled diagenesis governs reservoir quality in the carbonate Dehloran Field, southwest Iran. *Petroleum Geoscience*, **12**: 115–126.
- Tucker, M.E., 2001. *Sedimentary Petrology: An Introduction to the Origin of Sedimentary Rocks*. Blackwell Scientific Publications.
- Tucker, M.E., Wright, V.P., 1990. *Carbonate Sedimentology*. Blackwell Scientific Publications (Oxford).
- Veizer, J., 1983. Trace elements and isotopes in sedimentary carbonates. *Reviews in Mineralogy*, **11**: 265–300.
- Veizer, J., Demovic, R., 1973. Environmental and climatic controlled fractionation of elements in the Mesozoic carbonate sequence of the western Carpathians. *Sedimentary Petrology*, **43**: 258–271.
- Veizer, J., Hoefs, J., 1976. The nature of  $O^{18}/O^{16}$  and  $C^{13}/C^{12}$  secular trends in sedimentary carbonate rocks. *Geochimica et Cosmochimica Acta*, **40**: 1387–1395.
- Veizer, J., Mackenzie, F.T., 2014. Evolution of sedimentary rocks. *Treatise on Geochemistry*, **7**: 399–435.
- Veizer, J., Ala, D., Azmy, K., Bruckschen, P., Buhl, D., Bruhn, F., Carden, G.A.F., Diener, A., Ebner, S., Goddard, Y., Jasper, T., Korte, C., Pawellek, F., Podlaha, O.G., Strauss, H., 1999.  $^{87}Sr/^{86}Sr$ ,  $\delta^{18}O$  and  $\delta^{13}C$  evolution of Phanerozoic seawater. *Chemical Geology*, **161**: 59–88.
- Vincent, B., Rambeau, C., Emmanuel, L., Loreau, J.P., 2006. Sedimentology and trace element geochemistry of shallow marine carbonates: an approach to paleoenvironment analysis along the Pagny-sur-Meuse section (Upper Jurassic, France). *Facies*, **52**: 69–84.
- Vincent, B., Van Buchem, F.S.P., Bulot, L.G., Immenhauser, A., Caron, M., Baghbani, D., Huc, A.Y., 2010. Carbon isotope stratigraphy and organic matter distribution in the Aptian–Lower Albian successions of southwest Iran (Dariyan and Kazhdumi Formation). *GeoArabia*, **4**: 139–197.
- Winefield, P.R., Nelson, C.S., Hodder, A.P.W., 1996. Discriminating temperate carbonates and their diagenetic environments using bulk elemental geochemistry: a reconnaissance study based on New Zealand Cenozoic limestones. *Carbonates and Evaporites*, **11**: 19–31.
- Zhang, X., Wang, Y., Chen, X., 2000. Diagenesis and porosity of the Cambrian-Ordovician carbonate shoal facies at Yangjiaping, Shimen, Hunan. *Acta Geologica Sinica*, **74**: 29–45.